



## OPEN ACCESS

## EDITED BY

Fang-Zhen Teng,  
University of Washington, United States

## REVIEWED BY

Hossein Kouhestani,  
University of Zanjan, Iran  
Ryan Mathur,  
Juniata College, United States

## \*CORRESPONDENCE

Runsheng Han,  
554670042@qq.com

## SPECIALTY SECTION

This article was submitted  
to Geochemistry,  
a section of the journal  
Frontiers in Earth Science

RECEIVED 26 April 2022

ACCEPTED 15 August 2022

PUBLISHED 09 September 2022

## CITATION

Li L, Han R, Zhang Y, Wu J and Feng Z  
(2022), Trace element signatures of  
sphalerite in the Sichuan Daliangzi Ge-  
rich Pb-Zn deposit and its implications  
for deep ore prospecting.  
*Front. Earth Sci.* 10:928738.  
doi: 10.3389/feart.2022.928738

## COPYRIGHT

© 2022 Li, Han, Zhang, Wu and Feng.  
This is an open-access article  
distributed under the terms of the  
[Creative Commons Attribution License  
\(CC BY\)](https://creativecommons.org/licenses/by/4.0/). The use, distribution or  
reproduction in other forums is  
permitted, provided the original  
author(s) and the copyright owner(s) are  
credited and that the original  
publication in this journal is cited, in  
accordance with accepted academic  
practice. No use, distribution or  
reproduction is permitted which does  
not comply with these terms.

# Trace element signatures of sphalerite in the Sichuan Daliangzi Ge-rich Pb-Zn deposit and its implications for deep ore prospecting

Lingjie Li<sup>1</sup>, Runsheng Han<sup>1\*</sup>, Yan Zhang<sup>1</sup>, Jianbiao Wu<sup>1</sup> and Zhixing Feng<sup>2</sup>

<sup>1</sup>Faculty of Land Resource Engineering, Kunming University of Science and Technology, Kunming, China, <sup>2</sup>Sichuan Huidong Daliang Mining Co. Ltd., Xichang, China

The Daliangzi Pb-Zn deposit is one of the typical Ge-rich Pb-Zn deposits in the Sichuan-Yunnan-Guizhou Pb-Zn polymetallic metallogenic triangle area (SYGT), with its Pb, Zn, and Cd reserves reaching the scale of a large-sized deposit and its Ge reserve reaching that of a medium-sized deposit. Based on LA-ICP-MS *in-situ* analysis in combination with element mapping, this study reveals the occurrence state of trace elements and ore-forming temperature of sphalerite in ores. The study shows that the sphalerite in the deposit is characterized by rich Cd, Ge, and Ga, relatively rich Fe, very variable Cu and Pb contents, and poor Mn, In, and Sn. This data indicates that Cd, Mn, Fe, and Pb occur in sphalerite in the form of isomorphism or locally in the form of microinclusions in galena. Good correlation between Cu(Ag) and Ge and that between (Cu+Ag) and (Ga+As+Sb) suggest that the substitution relationship with Zn is  $n\text{Cu}^{2+} + \text{Ge}^{2+} \leftrightarrow (n+1)\text{Zn}^{2+}$  or  $n(\text{Cu}, \text{Ag})^{2+} + \text{Ge}^{2+} \leftrightarrow (n+1)\text{Zn}^{2+}$  and  $(\text{Cu} + \text{Ag})^{1+} + (\text{Ga} + \text{As} + \text{Sb})^{3+} \leftrightarrow 2\text{Zn}^{2+}$ , and chalcopyrite and Ge, Ga, and Ga-rich microinclusions exist locally; the contents of Ge, Cd, Cu, Pb, Fe, Mn, and other elements in brown yellow sphalerite are higher than those in light yellow sphalerite while Ga and In are relatively more enriched in the latter. The estimation by GGIMFis geothermometer and the trace element signature of the sphalerite indicates that the temperature of the deposit is low-moderate: the formation temperature of the sphalerite in stage II is 86–213°C (134°C on average) ~ 106–238°C (170°C on average) and that in stage III is 88–105°C (96°C on average) ~ 134–147°C (140°C on average), demonstrating that the precipitation mechanism of ore-forming elements is the drop in fluid temperature. Based on this, an ore-forming model of the deposit has been established, and it is believed that the ore district has potential for deep prospecting of Cu, Pb, Zn, and other metal resources.

## KEYWORDS

key metallic elements in sphalerite, metallogenic model of deposit, potential for deep prospecting, Daliangzi Pb-Zn deposit, Southwest Sichuan

## Introduction

As the major ore mineral of Pb-Zn deposit, sphalerite contains many trace elements such as Fe, Cd, Ga, Ge, In, and Se (Liu et al., 1984; Tu et al., 2003; Ishihara et al., 2006; Wang et al., 2010; Belissont et al., 2014), the composition of which can reflect the composition and physical and chemical conditions of ore-forming fluid, thus providing a theoretical basis for discussing ore-forming process (Zhang, 1987; Tu et al., 2003; Li et al., 2016; Wu et al., 2019; Hu et al., 2019). The former research studies have indicated that  $Zn^{2+}$  in sphalerite can be replaced by other positive ions with similar electrovalence and radius (e.g.,  $Pb^{2+}$ ,  $Cd^{2+}$ ,  $Co^{2+}$ , and  $Ge^{2+}$ ) (Cook et al., 2009) or by coupling (e.g.,  $2Zn^{2+} \leftrightarrow Ge^{4+} + 2(Cu^+, Ag^+)$ ,  $2Zn^{2+} \leftrightarrow Cu^+ + In^{3+}$ ) (Wu et al., 2019). In addition, as the content of trace elements in sphalerite is related to ore-forming temperature, former researchers have used Ga/Ge ratio instead of a geothermometer to represent ore-forming temperature (Möller et al., 1987); when studying sea bottom spout depositional type (VHMS) Pb-Zn deposit, Keith et al. (2014) thought that fractionation effect existed in sphalerite under the influence of  $f_{S_2}$  and  $f_{O_2}$  of ore-forming fluid and used the Fe/Zn ratio of sphalerite instead of geothermometer to represent ore-forming temperature; Frenzel et al. (2016), according to the contents of Fe, Mn, Ga, Ge, and In in sphalerite, established sphalerite geothermometer (GGIMFis) by principal component analysis; Mondillo et al. (2018) and (Wei et al., 2018a) used sphalerite geothermometer (GGIMFis) to estimate the ore-forming temperature of deposit. The former researchers have mostly used electron microprobe analysis (EMPA) or inductively coupled plasma mass spectrometry (ICP-MS) to measure trace elements of sphalerite, but the study on temperature tracing of trace elements has been constrained to some extent by detection limit and test accuracy. In recent years, however, the development of *in-situ* micro-area trace element testing technique, laser ablation inductively coupled plasma mass spectrometry (LA-ICP-MS), has made it possible to reveal the trace element signature of sphalerite in different types of Pb-Zn deposits, effectively explain the occurrence characteristics of trace elements in sphalerite (Cook et al., 2009; Ye et al., 2011), and represent in details the physical and chemical conditions for the formation of deposit and identify the genesis of mineral deposit.

Located within the southwest margin of the Yangtze block (Figure 1), Sichuan-Yunnan-Guizhou Pb-Zn polymetallic metallogenic domain is an important part of the large-area low-temperature metallogenic domain in southwest China. At present, over 500 Pb-Zn deposits (ore spots) with carbonate as host rock have been found in this area (Liu et al., 1999; Cui et al., 2018), including more than 10 large and super-large Pb-Zn

deposits (Huize, Chipu, Maozu, Maoping, Lehong, Maliping, Fule, Nayongzhi, Zhugongtang, Daliangzi, Tianbaoshan, etc.) (Ye et al., 2011; Wang et al., 2013; Han et al., 2014; Hu et al., 2017a; Cui et al., 2018). The Pb-Zn deposits in this area have typical characteristics of the epigenetic deposits, with the lithology of ore-host strata, mineral assemblage, and wall rock alteration basically the same as those of typical MVT Pb-Zn deposit (Han et al., 2006; Han et al., 2007b; Jin, 2008; Wu, 2013; Zhang et al., 2015), but the geological setting of ore-forming processes, characteristics of the ore-forming fluid, mode of action of ore-forming, and rules of occurrence of ore body different from those of typical MVT Pb-Zn deposit (Huang et al., 2004; Han et al., 2007b; Han et al., 2020). In addition, this area is one of the world's major areas with ultra-normal enrichment of rare and dispersed elements and an important production base of critical metals of China, with 21 and 8% global Ga and Ge reserves respectively (Wen et al., 2019). The Daliangzi Pb-Zn deposit is one of the typical large deposits in this metallogenic domain and a typical carbonate-hosted epigenetic hydrothermal deposit. The Zn+Pb, Ge, and Cd reserves of the deposit exceed 900 thousand, 100, and 4,000 tons respectively. The former researchers believe that under obvious tectonic control, the deposit is closely related to the "black/fracture zone" (Wang et al., 2018; Han et al., 2020; Han et al., 2021; Kong et al., 2021). However, there is still great argument about the genesis of the deposit, and the major types of deposits are believed to include 1) lixiviation reworked deposit (Zeng et al., 1982), 2) paleokarst deposit (Wang et al., 1985), 3) hydrothermal lixiviation type deposit (Wang et al., 1991), 4) epigenetic low-intermediate temperature hydrothermal deposit (Lin, 1994), sedimentary-reworked strata-bound deposit (Zhu et al., 1994), 5) MVT Pb-Zn deposit (Li, 2003; Zhang et al., 2008; Zhou et al., 2008; Wu, 2013; Yuan et al., 2014; Zhang, 2015; Leach et al., 2019), and 6) HZT Pb-Zn deposit (Han et al., 2020). The former researchers who have studied *in-situ* trace elements of sulfide in partial deposits of Sichuan-Yunnan-Guizhou Pb-Zn polymetallic metallogenic domain (Ye et al., 2011; Ye et al., 2016; We et al., 2018, 2021) believe that rare and dispersed elements such as Ge, Ga, and Cd mainly exist in sphalerite while As and Sb mainly exist in galena (Ye et al., 2016), but there is still argument about the occurrence state of Ge, Ga, and other rare and dispersed elements in sphalerite, similarities and differences exist in composition of trace elements in sphalerite of different ore-concentrated areas in the metallogenic domain, and the research on how to control the enrichment of trace elements in the sphalerite during mineralization and its significance for mineral prospecting is relatively weak.

This study proposes to carry out systematic research on the

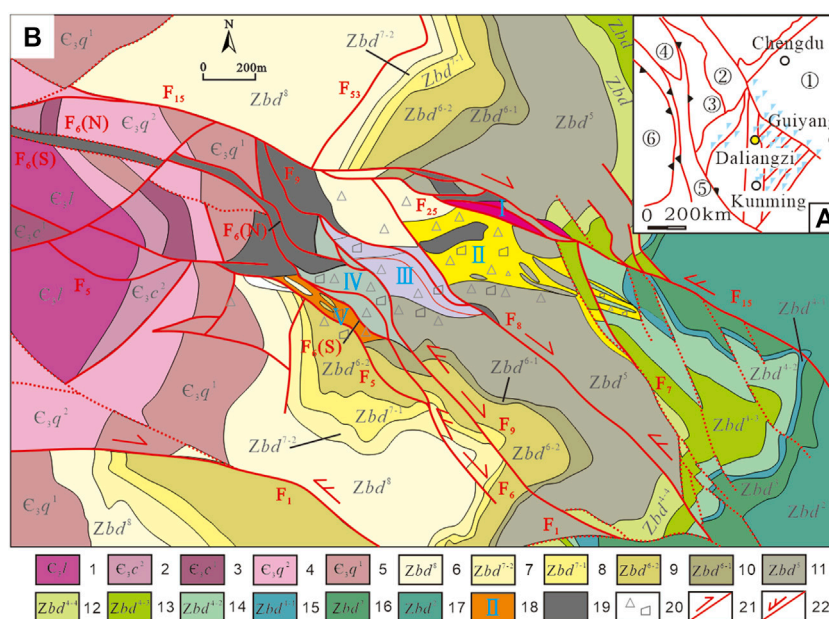


**FIGURE 1**  
 The map showing framework of the lead-zinc deposit in the Sichuan Yunnan and Gui zhou mineralization district, Geologic sketch map of the Daliangzi Germanium-rich Pb-Zn deposit (Modified after Wu et al., 2020). Notes: (A): ①-Yongtze Block; ②-Garzé Orogenic Belt; ③-Yidun Arc Collision-orogenic; ④-Lanping Block; ⑤-Sanjiang Collision-orogenic; ⑥-Indian Block; (B): 1- Lower Cambrian Longwangmiao formation, Dolomitic limestone; 2-Lower Cambrian Canglangpu formation, Argillaceous limestone; 3-Lower Cambrian Canglangpu formation, Quartz Sandstone; 4-Lower Cambrian Qiongzhusizu formation, Shale; 6-Lower Cambrian Qiongzhusizu formation, Quartz Sandstone; 7-Upper Sinian Dengying Formation, Section 8, Chert banded dolomite; 8-Upper Sinian Dengying Formation, Section 7<sup>1st</sup>, Phosphorous dolomite; 9-Upper Sinian Dengying Formation, Section 6<sup>2nd</sup>, Siliceous dolomite; 10-Upper Sinian Dengying Formation, Section 6<sup>1st</sup>, Banded dolomite; 11-Upper Sinian Dengying Formation, Section 5, Siliceous dolomite; 12-Upper Sinian Dengying Formation, Section 4<sup>4th</sup>, Chert nodule bearing siliceous dolomite; 13-Upper Sinian Dengying Formation, Section 4<sup>3rd</sup>, Argillaceous dolomite; 14-Upper Sinian Dengying Formation, Section 4<sup>2nd</sup>, Sandy dolomite; 15-Upper Sinian Dengying Formation, Section 4<sup>1st</sup>, Chert; 16-Upper Sinian Dengying Formation, Section 3, Argillaceous dolomite; 17-Upper Sinian Dengying Formation, Section 2, Dolomite; 18-Ore body and Number; 19-“Black/fracture zone”; 20-Breccia; 21-Fault and movement direction in metallogenic period; 22-Fault and movement direction in the later stage of mineralization.

composition of trace elements of sphalerite at different stages in the Daliangzi Pb-Zn deposit to find out their distribution characteristics and reveal their occurrence state, use GGMIF is a geothermometer to estimate the ore-forming temperature of the deposit at different stages of mineralization, further discuss the ore-forming process, and establish the ore-forming model, thus providing a theoretical basis for mineral prospecting.

### Geology of the deposit

The Daliangzi Pb-Zn deposit is situated on the west side of the Ganluo-Xiaojiang fault on the southwest margin of the Yangtze block (Figure 1A). The stratum in the area is composed of fold basement and sedimentary cover, the former mainly consisting of Archean-Paleoproterozoic mesometamorphic complexes, Mesoproterozoic metamorphic fine clastic rocks intercalated with metamorphic volcanic sedimentary rocks, and Neoproterozoic epimetamorphic fine clastic rocks and carbonate rocks, and the latter mainly

consisting of Upper Sinian, Cambrian, Ordovician, and Lower Permian marine carbonate rocks and fine clastic rocks, Upper Permian Emeishan basalts, and Mesozoic continental red beds.

Fault structures are extremely well-developed in this area, mostly in the S-N direction, forming a left-column “xi-type structure”. The main structures include the Anninghe fault, Ganluo-Xiaojiang fault, Zhaotong-Qujing buried fault, and N-E direction bundle of folds (Liu et al., 1999; Han et al., 2006; Zhang et al., 2006). These deep-seated faults to the depth of the basement with multi-stage tectonic activities have not only controlled the distribution of lithofacies in the region but created favorable conditions for the migration of regional ore-forming fluid and the formation of Pb-Zn deposits (Han et al., 2006).

The main exposed strata in the area (Figure 1B) are Upper Sinian Dengying Formation (Zbd), Lower Cambrian Qiongzhusi Formation (€1q), Canglangpu Formation (€1c), and Longwangmiao Formation (€1l), and Quaternary residual slope sediments (Q). Upper Sinian Dengying Formation (Zbd) is the major ore-bearing stratum mainly composed of dolomite. The ore area is in the east wind of the Daqiao multiple syncline

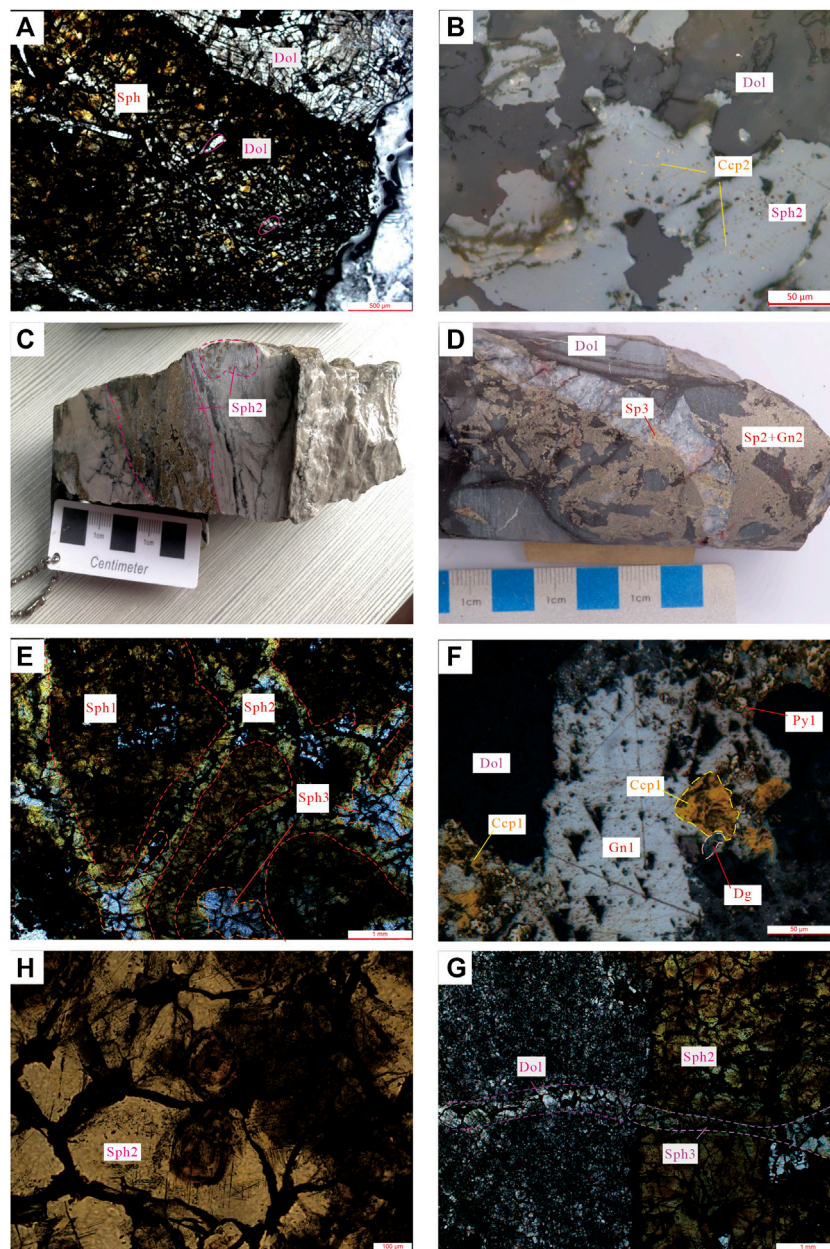


**FIGURE 2**

Microphotographs of ores of different stages in the Daliangzi Pb-Zn deposit. (A) Dolomite breccia cemented by sphalerite and galena, Sph 2 is filled along Sph 1 particle edge and between cracks; (B) Sph 2:Sph2: mesh-vein and star point Brown - yellowish brown sphalerite; (C) Gn 1 replaced or enclose Py 1 and Ccp 1, Py 1 replaced or enclose Ccp 1; (D) Sph 2: banded sphalerite; (E) Sph 2: sphalerite present a solid solution decomposition structure; (F) Sph 3 vein replaces early Dol and then crosscuts the Sp2; (G) Sph 2 is filled along sph1 particles, Sph3 is filled along sph2 particles; (H) sphalerite replaced or enclose calcite. Sph-sphalerite; Gn-Galena; Ccp-Chalcopyrite; Py-Pyrite; Dg-Digenite; And-Anglesite; Dol-Dolomite.

structure which moves towards nearly S-N direction; subsidiary anticline towards NE-NNE direction also develops in the area. Fault structures developing in the area can be divided into four grades (Wu et al., 2021): the first-grade structures are F1, F2, F13, F15, and F64 in NWW- nearly E-W direction, which controls the distribution of deposits; the second-grade structures are the series

of N-W direction faults (F3, F8, F6, F100, and F5) derived from the first-grade structures; the third-grade structures are secondary and interlayer fault zones, which control individual ore bodies (blocks); and the fourth-grade structures are sub-secondary faults and joint fissures, which control the shape and the occurrence of the ore-bearing vein.

Mineral	Hydrothermal Stage			Supergene Oxidization
	Stage I	Stage II	Stage III	
Pyrite	————	————	————	
Sphalerite	————	————	————	
Galena	————	————	————	
Chalcopyrite	————	————		
Arsenopyrite	————	————		
Marcasite	————			
Freibergite		————	————	
Pyrargyrite		————	————	
Quartz	————		————	
Chalcedony				————
Dolomite	————	————	————	————
Calcite		————	————	————
Asphalt	————			
Smithsonite				————
Cerussite				————
Greenockite				————
Malachite				————
Digenite				————
Limonite				————

FIGURE 3

Metallogenic period, metallogenic stage, and mineral forming sequence of Daliangzi lead-zinc deposit.

Ore bodies are controlled by both structure (fault and “black/fracture zone”) and lithology. “Black/fracture zone” is the major ore-bearing structure, and is controlled by NW and NWW-direction faults together with ore bodies. Ore bodies move towards the NW direction overall and tend to NE or locally SW by 56°–88° (Figure 1B), with a length of approximately 630 m and an average thickness of 52.67 m. Ore bodies are chimney-like, lenticular, and sack-like, and their mineralization weakens from center to edge. Ore minerals mainly include sphalerite, galena, pyrite, and chalcopyrite while gangue minerals mainly include dolomite, calcite, quartz, and chalcedony. Ores are mainly of panidiomorphic-hypidiomorphic, granular, metasomatic relict texture (Figure 2A) or solid solution decomposition texture

(Figure 2A), and mainly of massive, brecciated, mesh-vein structure (Figures 2B) or vein structure. Wall-rock alteration in the area is relatively weak, mainly including carbonatation, silicification, pyritization, and carbonization.

According to the paragenetic assemblage, texture and structure, and crosscutting relation of minerals, ore forming of The Daliangzi Pb-Zn deposit can be divided into two processes, i.e., 1) hydrothermal mineralization (Figure 3), which can be divided into three stages: in stage I, sphalerite is dark brown or brownish black xenomorphic-hypidiomorphic granular aggregate in a symbiosis with xenomorphic granular galena (Figure 2E), and it can be seen locally that chalcopyrite, pyrite, and galena present an edge-sharing structure (Figure

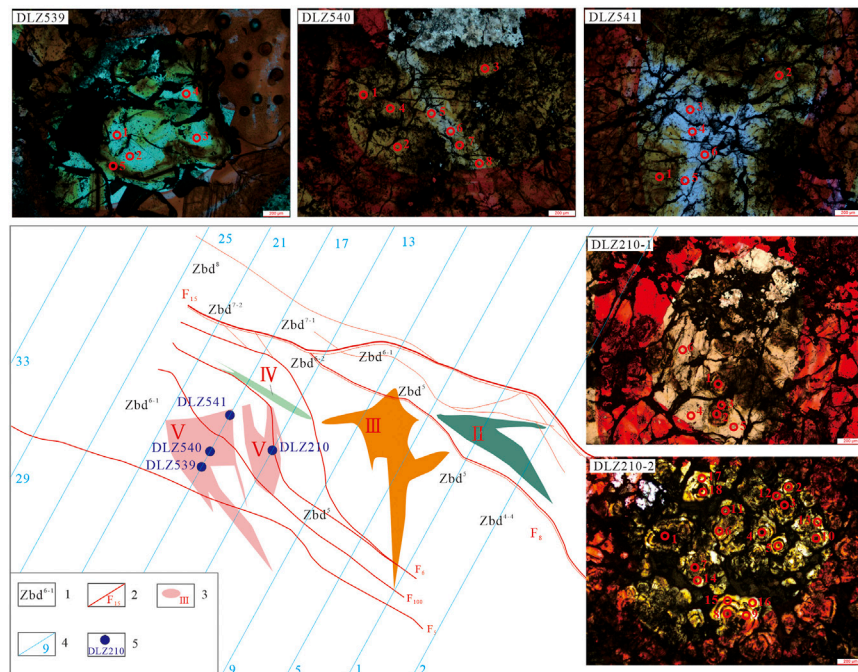


**FIGURE 4**

The sampling location map and the LA-ICP-MS analysis points of the Daliangzi Lead-Zinc deposit 1-Stratum number; 2-Fault and number; 3-Ore body and Number; 4-Exploration line and number; 5-Sampling point location and number.

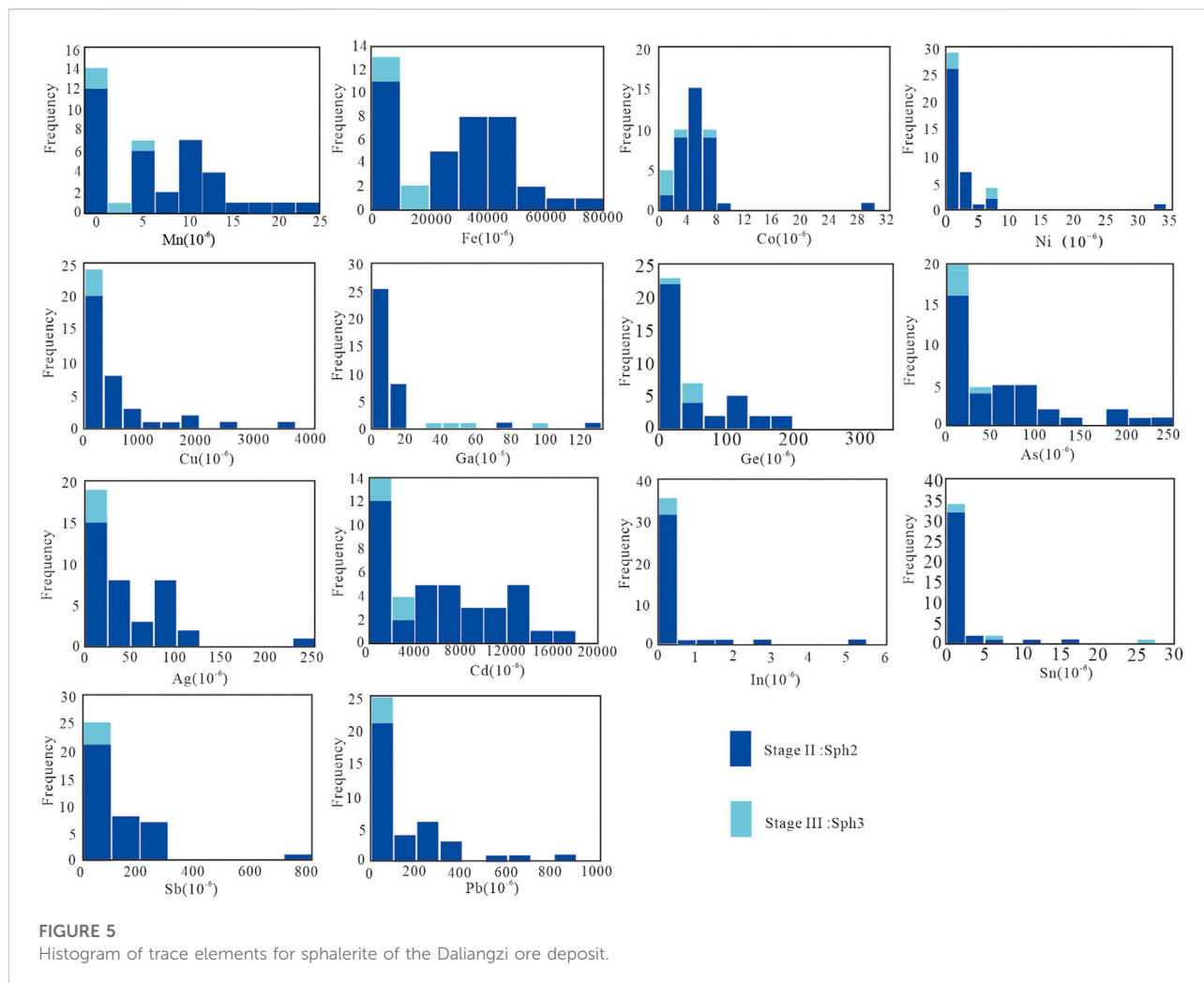
2F); in stage II, sphalerite is dark brown or pale brown, has a coarsely granular structure, and presents a block, vein or star point shape (Figures 2C,D), often filling in sphalerite particles and fissures of stage I (Figure 2E), and banded sphalerite can be seen locally (Figure 2H) and developed chalcopyrite and sphalerite present a solid solution decomposition structure (Figure 2B); in stage III, sphalerite occurs as extra-thin veins, replacing dolomite veins of earlier stage and cutting through sphalerite of Stage II (Figure 2G, and 2) hypergenesis, where bonamite, vanadinite, digenite, malachite, etc. take shape.

## Sampling and analytical test method

Ore samples from the Daliangzi Zn-Pb deposit were collected from orebody V (Figure 4). Trace element analysis of minerals was conducted by LA-ICP-MS at the Wuhan SampleSolution Analytical Technology Co., Ltd., Wuhan, China. Detailed operating conditions for the laser ablation system and the ICP-MS instrument and data reduction are the same as the description made by Zong et al. (2017). Laser sampling was performed using a GeolasPro laser ablation system that consists of a COMPexPro 102 ArF excimer laser (wavelength of 193 nm and maximum energy of 200 mJ) and a MicroLas optical system. An Agilent 7700e ICP-MS instrument was used to acquire ion-signal intensities. Helium was applied as a carrier gas. Argon was used as the make-up gas and mixed with the

carrier gas via a T-connector before entering the ICP. A “wire” signal smoothing device is included in this laser ablation system (Hu et al., 2015). The spot size and frequency of the laser were set to 32  $\mu\text{m}$  and 50Hz, respectively, in this study. Trace element compositions of minerals were calibrated against various reference materials (BHVO-2G, BCR-2G, and BIR-1G) without using an internal standard (Liu et al., 2008). Each analysis incorporated a background acquisition of approximately 20–30 s followed by 50 s of data acquisition from the sample. An Excel-based software ICPMSDataCal was used to perform off-line selection and integration of background and analyzed signals, time-drift correction, and quantitative calibration for trace element analysis (Liu et al., 2008).

Stage II is the main metallogenic stage, So we selected the banded sphalerite in the II stage of hydrothermal mineralization. Trace elements of sphalerite were determined using an NWR 193 nm ArF Excimer laser-ablation system coupled to an iCAP RQ (ICPMS) at the Guangzhou Tuoyan Analytical Technology Co., Ltd., Guangzhou, China. The ICP-MS was tuned using NIST 610 standard glass to yield low oxide production rates. 0.7 L/min He carrier gas was fed into the cup, and the aerosol was subsequently mixed with 0.89 L/min Ar make-up gas. The laser fluence was 5 J/cm<sup>2</sup>, with a repetition rate of 20 Hz and a 5 or 10  $\mu\text{m}$  spot size. The laser scan speed was 20  $\mu\text{m/s}$ . The raw isotope data were reduced using the “TRACE ELEMENTS” data reduction scheme (DRS). The DRS runs within the freeware



IOLITE package of Paton et al. (2011). In IOLITE, user-defined time intervals are established for the baseline correction procedure to calculate session-wide baseline-corrected values for each isotope.

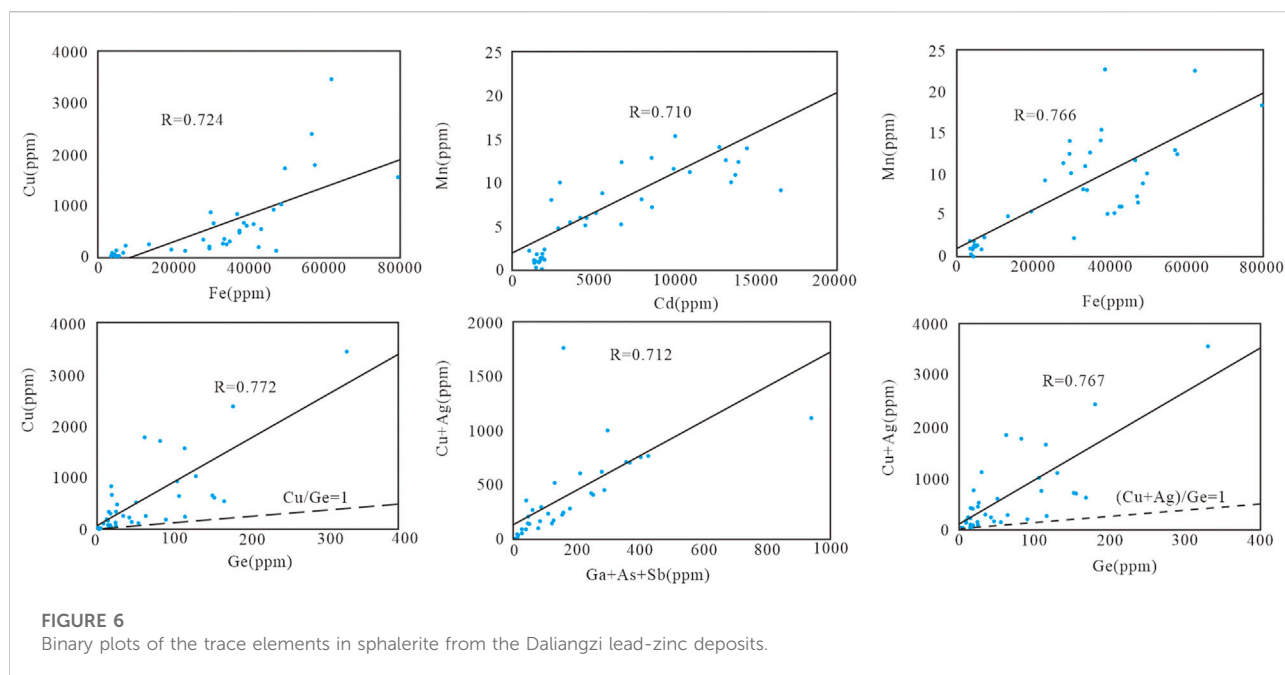
## Test results

The sphalerite of this deposit is mostly dark brown or brownish-black sphalerite of stage II with 0.4–6.1% Fe. From stage II to stage III, the contents of all trace elements but Ga of the sphalerite decrease gradually (Figure 5). The characteristics of the sphalerite are as follows:

1) The Fe content is high while the Mn content is low. From stage II to stage III of mineralization, both Fe and Mn contents decrease gradually (Figure 5), presenting a positive correlation (correlation coefficient  $R=0.766$ ) (Figure 6). The Fe content in stage II and that in stage III

is  $3,489.08 \times 10^{-6} \sim 79,574.78 \times 10^{-6}$  ( $30,494.46 \times 10^{-6}$  on average) and  $4,688.77 \times 10^{-6} \sim 19,355.93 \times 10^{-6}$  ( $11,178.39 \times 10^{-6}$  on average), respectively; the Mn content in stage II and that in stage III are  $0.06 \times 10^{-6} \sim 22.59 \times 10^{-6}$  ( $7.95 \times 10^{-6}$  on average) and  $1.82 \times 10^{-6} \sim 5.45 \times 10^{-6}$  ( $3.60 \times 10^{-6}$  on average), respectively.

2) Among rare and dispersed elements, Cd, Ge, and Ga are the most enriched while the contents of Se, In, Tl, and Te are relatively low. From stage II to stage III, the contents of Cd and Ge decrease gradually while that of Ga increases gradually (Figure 5). The content of Cd in stage II and that in stage III are  $967.87 \times 10^{-6} \sim 16,548.51 \times 10^{-6}$  ( $6,426.31 \times 10^{-6}$  on average) and  $1,801.72 \times 10^{-6} \sim 3,523.68 \times 10^{-6}$  ( $2,511.80 \times 10^{-6}$  on average), respectively (Figure 5), and the content of Cd and that of Mn present a positive correlation (correlation coefficient  $R = 0.710$ ) (Figure 6); The content of Ge in stage II and that in stage III are  $0.38 \times 10^{-6} \sim 331.20 \times 10^{-6}$  ( $61.79 \times 10^{-6}$  on average) and  $24.15 \times 10^{-6} \sim 64.26 \times 10^{-6}$  ( $44.26 \times 10^{-6}$  on average), respectively (Figure 5), and the content of



Ge and those of Cu and Cu+Ag present a positive correlation (correlation coefficients  $R = 0.772$  and  $0.767$ , respectively) (Figure 6); the content of Ga at stage II and that at stage III are  $0.03 \times 10^{-6}$ – $124.11 \times 10^{-6}$  ( $11.49 \times 10^{-6}$  on average) and  $30.79 \times 10^{-6}$ – $93.81 \times 10^{-6}$  ( $56.70 \times 10^{-6}$  on average), respectively (Figure 5); the contents of such rare and dispersed elements as Se, In, Tl, and Te are relatively low, with values obtained from some of the measurement points lower than the detection limit.

- 3) Cu, Pb, Ag, and Co are enriched, but their contents change within a wide range. From stage II to stage III, Cu, Pb, Ag, and Co contents all decrease gradually. The content of Cu in stage II and that in stage III are  $3.51 \times 10^{-6}$ – $3,448.3 \times 10^{-6}$  ( $563.63 \times 10^{-6}$  on average) and  $132.47 \times 10^{-6}$ – $258.68 \times 10^{-6}$  ( $192.10 \times 10^{-6}$  on average), respectively (Figure 5), of which most values are lower than  $1,000 \times 10^{-6}$  except for individual exceptional high value caused by microinclusion of chalcopyrite (or copper-bearing sulfide) contained in the sphalerite (Figure 2E); the content of Pb in stage II and that in stage III are  $0.27 \times 10^{-6}$ – $596.18 \times 10^{-6}$  ( $145.94 \times 10^{-6}$  on average) and  $4.61 \times 10^{-6}$ – $12.87 \times 10^{-6}$  ( $9.19 \times 10^{-6}$  on average), respectively (Figure 5), of which most values are lower than  $400 \times 10^{-6}$  except for individual exceptional high value caused by microinclusion of galena contained therein (Figures 7, 8); the content of Ag in stage II and that in stage III are  $0.74 \times 10^{-6}$ – $237.12 \times 10^{-6}$  ( $48.20 \times 10^{-6}$  on average) and  $13.20 \times 10^{-6}$ – $22.41 \times 10^{-6}$  ( $17.36 \times 10^{-6}$  on average), with a strong positive correlation between Cu+Ag and Ga+As+Sb (correlation coefficient  $R = 0.712$ ); the content of Co in stage II and that in stage III are  $0.7 \times$

$10^{-6}$ – $28.6 \times 10^{-6}$  ( $5.45 \times 10^{-6}$  on average) and  $0.48 \times 10^{-6}$ – $2.89 \times 10^{-6}$  ( $1.46 \times 10^{-6}$  on average), respectively (Figure 5).

- 4) The As and Sb contents are high. The content of As in stage II and that in stage III are  $0.32 \times 10^{-6}$ – $229.77 \times 10^{-6}$  ( $57.87 \times 10^{-6}$  on average) and  $0.00 \times 10^{-6}$ – $39.57 \times 10^{-6}$  ( $19.67 \times 10^{-6}$  on average), respectively (Figure 5); the content of Sb in stage II and that in stage III are  $0.19 \times 10^{-6}$ – $708.36 \times 10^{-6}$  ( $109.56 \times 10^{-6}$ ) and  $33.94 \times 10^{-6}$ – $76.27 \times 10^{-6}$  ( $57.03 \times 10^{-6}$  on average) (Figure 5); Ni and Sn contents are relatively low, both  $n \times 10^{-6}$ , with values obtained from some of the measurement points lower than the detection limit.

## Discussion

### Occurrence state of trace elements in sphalerite

Compared with conventional analysis methods such as electronic probes, LA-ICP-MS has higher accuracy, and in combination with the time resolution curve and mapping analysis feature, the occurrence state of trace elements can be better identified (Cook et al., 2009; Ye et al., 2011; George et al., 2015, 2016; Ye et al., 2016; Wu et al., 2019).

As far as the trace elements in the sphalerite of the deposit are concerned, Fe and Mn contents change within a wide range and present a positive correlation (correlation coefficient  $R = 0.766$ ); in addition, in the LA-ICP-MS time cross-section (Figure 8, 210-1-1# and 210-2-13# samples), their change trend, presented as a smooth

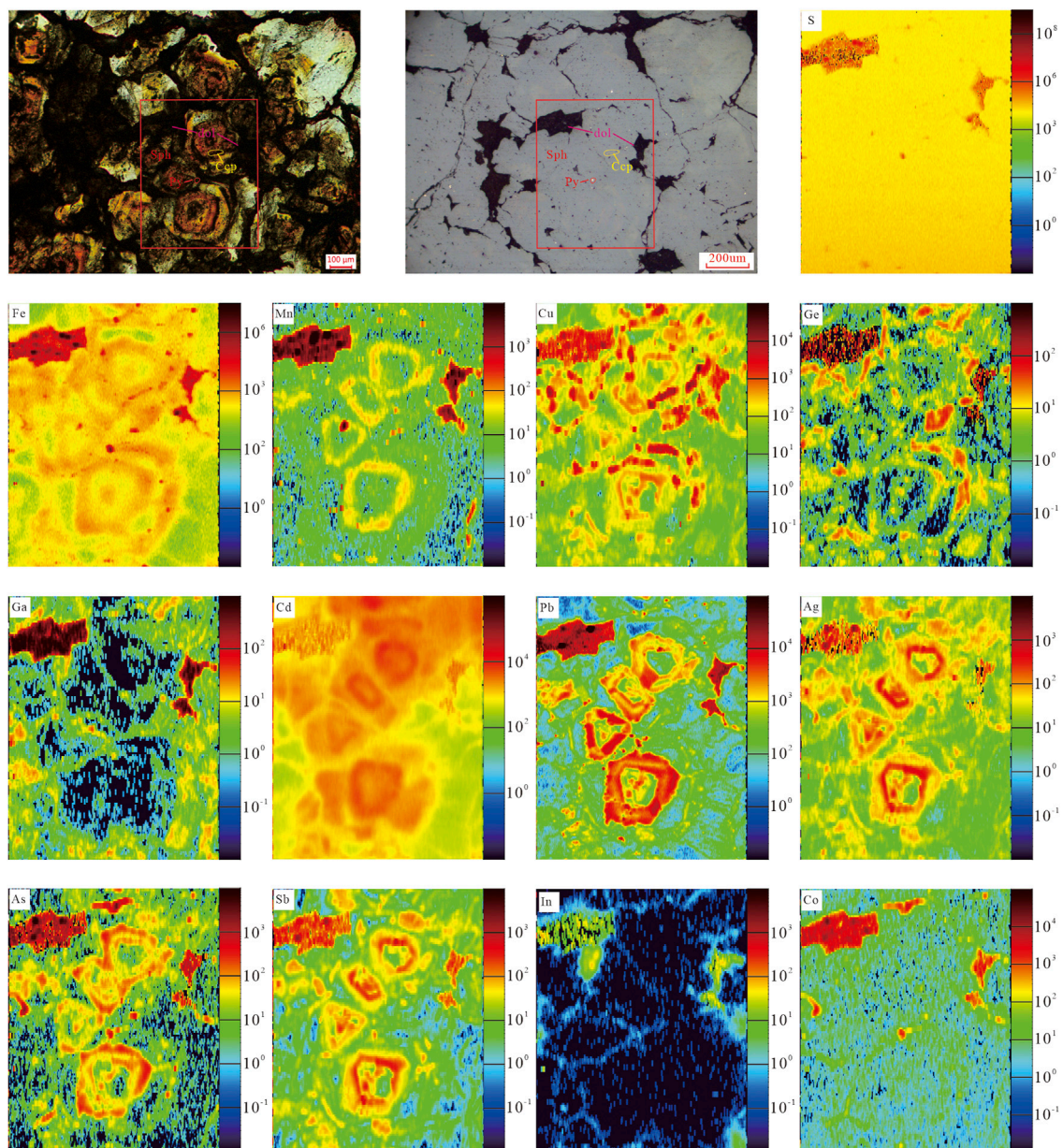


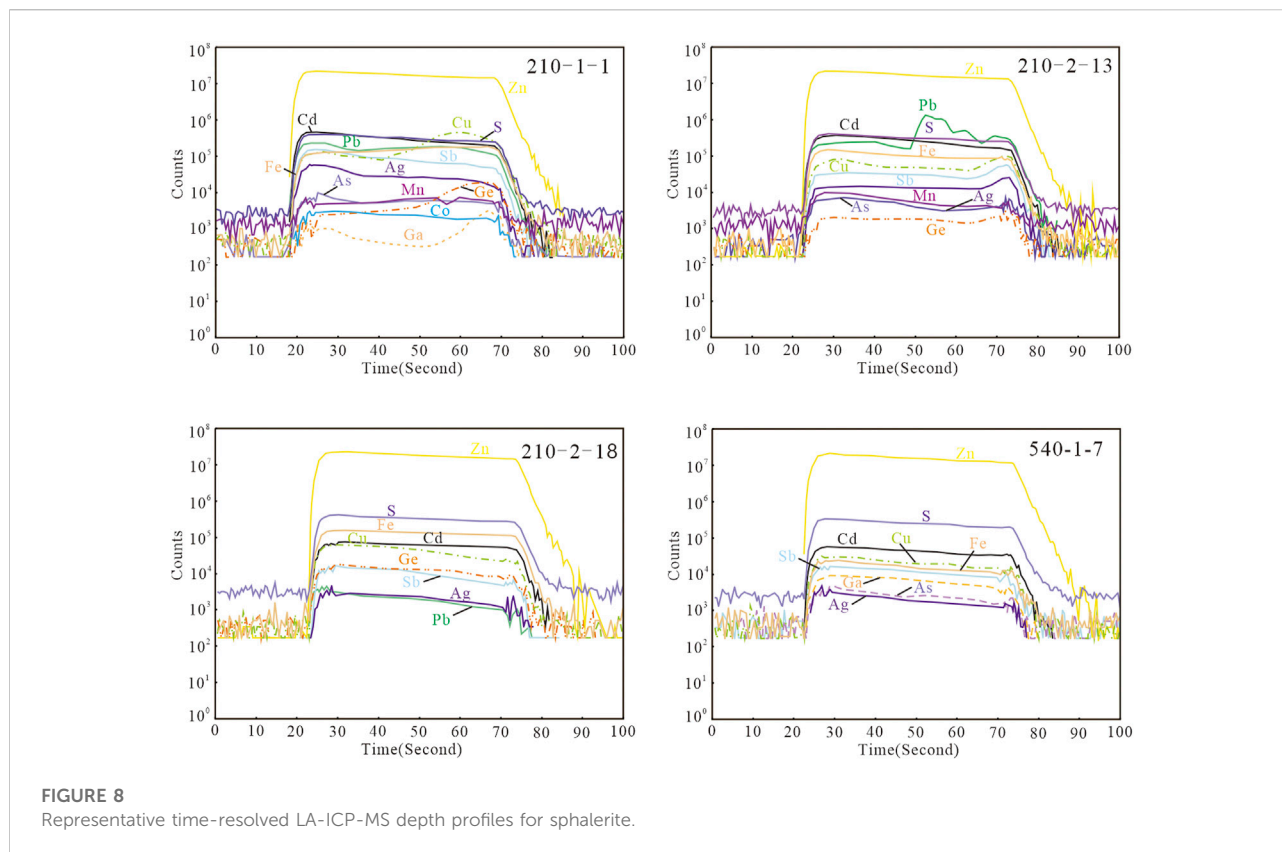
**FIGURE 7**  
Mapping images of sphalerite of the Daliangzi ore deposit. Scales in counts-per-second.

curve, is consistent with that of Zn and S contents; in mapping diagram (Figure 7), Fe and Mn contents of pale brown part of banded sphalerite are obviously higher than those in pale yellow sphalerite, and the exceptional local enrichment of Fe and Mn is probably caused by the microinclusions in pyrite. It shows that the majority of these two elements exist in sphalerite mainly in the form of isomorphism ( $\text{Fe}^{2+} \leftrightarrow \text{Zn}^{2+}$  or  $\text{Mn}^{2+} \leftrightarrow \text{Zn}^{2+}$ ) and the minority of them exist in the form of independent microinclusions.

Cd is one of the elements of which the content is high in the Daliangzi Pb-Zn deposit, and its content changes within a wide

range and does not present a normal distribution in the trace element diagram (Figure 5); in all LA-ICP-MS time cross-sections (Figure 8), its change trend, presented as a smooth curve, is consistent with that of Zn and S contents; in mapping diagram (Figure 7), Cd content of pale brown part of banded sphalerite is obviously higher than that in pale yellow sphalerite, and no exceptional enrichment can be seen. It shows that Cd exists in sphalerite in the form of isomorphism ( $\text{Cd}^{2+} \leftrightarrow \text{Zn}^{2+}$ ).

Co content is relatively high and presents a normal distribution in the trace element diagram (Figure 5); in representative time-



resolved LA-ICP-MS depth profiles (Figure 8, 201-1# sample), its change trend, presented as a smooth curve, is consistent with that of Zn and S contents; in mapping diagram (Figure 7), Co content of pale brown annulus in banded sphalerite is obviously higher than that in pale yellow sphalerite, and no exceptional enrichment can be seen. It shows that Co exists in sphalerite in the form of isomorphism ( $\text{Co}^{2+} \leftrightarrow \text{Zn}^{2+}$ ).

Sphalerite is rich in and the main carrier of Ge, and the occurrence mechanism of Ge in sphalerite has been a hot spot. Some scholars believe that  $\text{Ge}^{2+}$  enters sphalerite in place of  $\text{Zn}^{2+}$  ( $\text{Ge}^{2+} \leftrightarrow \text{Zn}^{2+}$ ) (Cook et al., 2009). Belissont et al. (2016) proposed the substitution mechanism of  $\text{Ge}^{4+} + 2(\text{Cu}, \text{Ag}) \leftrightarrow 3\text{Zn}^{2+}$  according to the correlation of Ge with such monogeny as Cu (Ag); for sphalerite rich in Ge ( $\text{Ge}/\text{Cu} > 0.5$ ) or with no correlation between Ge and Cu, the probable substitution mechanism is  $\text{Ge}^{4+} + \square$  (crystal vacancy)  $\leftrightarrow 2\text{Zn}^{2+}$  (Cook et al., 2015; Bonnet et al., 2016). According to the fact that  $\text{Zn}^{2+}$ ,  $\text{Cu}^{2+}$ , and  $\text{Ge}^{2+}$  have a similar covalent radius of the tetrahedron and in combination with the characteristics of the LA-ICP-MS laser ablation curve, Ye (2016) proposes the substitution mechanism of  $n\text{Cu}^{2+} + \text{Ge}^{2+} \leftrightarrow (n+1)\text{Zn}^{2+}$ . Through analysis of microbeam X-ray absorption near edge structure, Bonnet (2016) proposed that Ge and Cu occur in sphalerite in their oxidation state, i.e.,  $\text{Ge}^{4+}$  and  $\text{Cu}^{+}$ . Most of the LA-ICP-MS measured sphalerite is rich in Ge

(Figure 5), and Ge has a positive correlation with Cu and  $\text{Cu} + \text{Ag}$  ( $\text{Cu}/\text{Ge} > 1$ ,  $(\text{Cu} + \text{Ag})/\text{Ge} > 1$ ); in representative time-resolved LA-ICP-MS depth profiles (Figure 8, 210-2-18# and 540-1-7# point), its change trend, presented as a smooth curve, is consistent with that of Zn and S contents, with abnormal peak values of Cu, Ge, and Ga contents occurring at individual denudation points; the changing trend of Zn and S contents presented as a smooth curve indicates the possible existence of mineral containing Cu, Ge, and Ga, but no previous research report has ever mentioned any mineral containing Cu, Ge, and Ga simultaneously (Ye et al., 2019), so further study is needed; in mapping diagram (Figure 7), relative enrichment of Ge, Cu, and Ag and local anomalous enrichment of Ge and Cu can be seen in the pale brown part of banded sphalerite, indicating the existence of microinclusions containing Cu and Ge. Therefore, the possible substitution mode Ge is  $n\text{Cu}^{2+} + \text{Ge}^{2+} \leftrightarrow (n+1)\text{Zn}^{2+}$  or  $n(\text{Cu}, \text{Ag})^{2+} + \text{Ge}^{2+} \leftrightarrow (n+1)\text{Zn}^{2+}$ .

Pb content changes within a wide range, and in most LA-ICP-MS time cross-sections (Figure 8, 210-1-1# and 210-2-18# points), the changing trend is presented as a smooth curve and consistent with that of Zn and S contents, with exceptional values of Pb content at individual points (Figure 8, 210-2-13# sample); in mapping diagram (Figure 7), Pb content in the pale brown part of banded sphalerite is obviously higher than that in the pale

TABLE 1 Trace element in sphalerite from the Daliangzi Pb-Zn deposits ( $\times 10^{-6}$ ).

	Mn	Fe	Co	Ni	Cu	Ga	As	Ag	Cd	In	Sn	Sb	Tl	Pb	Ge	Color	PC1	Tmin(°C)	Tmax(°C)
210-1-1	9.47	40,350.15	6.64	0.00	1,218.54	3.65	136.83	168.48	12,009.83	0.0362	0.81	355.37	1.61	336.09	64.30	Pale brown	1.06	132	168
210-1-2	10.04	49,487.45	28.61	32.21	1720.00	10.93	86.67	39.32	2,873.17	0.0621	0.59	61.03	0.38	55.33	83.31	Pale brown	1.28	119	158
210-1-3	8.15	33,094.88	6.15	2.48	268.12	5.80	26.26	27.84	7,945.80	0.2448	0.72	55.01	0.21	59.89	34.78	Pale brown	0.86	145	178
210-1-4	0.87	6,490.95	3.83	0.00	90.71	72.84	1.13	12.60	1,578.41	0.1160	0.57	3.09	0.01	5.82	14.52	Pale yellow	1.81	86	133
210-1-5	1.34	5,371.42	2.79	0.00	23.27	7.18	2.65	11.98	1811.01	0.0120	0.64	5.37	0.01	16.21	4.59	Pale yellow	1.22	123	161
210-1-6	0.06	4,311.11	2.36	0.88	49.06	14.51	2.75	10.43	1773.82	0.0062	0.50	8.20	0.00	2.52	18.29	Pale yellow	2.37	51	106
210-2-1	12.38	57,466.98	3.62	2.72	1793.21	2.92	134.19	44.39	6,685.87	0.1167	0.47	78.09	3.39	354.86	62.26	Brown black	0.81	148	180
210-2-10	22.42	61,972.06	4.12	3.03	3,448.33	21.90	175.19	97.03	7,647.31	0.7358	3.74	222.63	0.56	231.34	331.20	Brown black	1.30	118	157
210-2-11	22.59	38,626.88	5.88	1.84	668.49	1.46	214.93	98.39	9,270.01	-	0.56	206.65	5.18	656.27	19.47	Pale brown	△	△	△
210-2-12	11.22	27,774.02	8.59	7.06	343.96	2.60	110.46	81.38	10,922.28	0.1778	0.56	131.07	2.21	854.06	15.34	Pale brown	0.48	168	195
210-2-13	15.95	36,851.91	5.45	3.76	841.64	0.40	130.50	63.85	10,845.65	0.0981	0.64	75.93	4.00	346.91	18.53	Pale brown	0.10	192	213
210-2-14	15.41	37,451.74	6.44	0.96	485.67	1.20	70.68	32.90	10,019.70	0.0195	0.29	55.88	1.93	221.54	26.00	Pale brown	0.59	161	190
210-2-15	13.97	29,553.64	6.70	2.77	209.87	0.03	37.57	28.65	14,427.69	0.0100	0.51	70.96	0.44	156.47	11.82	Pale brown	-0.32	213	238
210-2-17	8.81	48,436.47	6.86	0.00	1,028.03	0.26	123.03	79.73	5,525.19	0.0132	0.70	128.31	0.86	184.39	130.19	Pale brown	0.76	151	182
210-2-16	8.05	34,028.85	2.06	0.92	255.96	4.09	12.56	11.96	2,352.95	0.0207	0.75	41.64	0.04	3.97	116.59	Pale brown	1.32	116	156
210-2-2	12.58	34,785.49	5.68	0.56	311.02	0.52	67.29	98.94	13,129.15	0.0135	0.72	182.35	0.73	226.33	17.57	Pale brown	0.41	173	199
210-2-18	12.42	29,490.50	5.92	2.14	180.46	0.54	43.94	44.91	13,924.69	0.0104	0.58	108.86	0.66	158.95	14.44	Pale brown	0.41	173	199
210-2-3	11.64	46,542.04	4.29	7.05	926.63	13.55	179.88	71.44	9,921.35	0.3022	1.30	101.90	2.41	264.37	105.94	Brown black	1.18	125	162
210-2-4	14.07	37,459.58	7.08	2.47	523.81	3.23	61.79	80.95	12,742.32	0.0120	0.77	144.29	0.84	202.72	51.29	Brown black	1.03	134	169
210-2-5	10.91	33,358.35	6.27	1.52	353.06	0.56	77.03	103.16	13,723.95	0.0012	0.57	207.10	0.69	234.61	24.93	Pale brown	0.79	149	181
210-2-6	9.14	23,105.05	5.51	0.06	124.62	0.77	36.88	45.76	16,548.51	0.0065	0.56	86.97	0.51	220.46	9.27	Pale brown	0.51	166	194
210-2-7	12.87	56,756.34	5.98	5.21	2,388.89	18.36	91.10	58.25	8,559.63	0.1925	2.28	117.99	0.99	109.37	180.50	Brown black	1.39	112	153
210-2-8	18.31	79,574.78	6.19	0.08	1,567.02	3.96	97.26	76.28	6,149.86	0.0077	0.69	172.14	1.78	223.99	115.27	Brown black	1.22	122	160
210-2-9	10.08	29,807.89	6.60	0.40	874.42	1.60	229.77	237.12	13,464.89	0.0050	0.65	708.36	1.68	596.18	30.04	Pale brown	0.93	141	174
539-1-1	1.36	4,570.08	4.35	2.15	3.51	0.70	0.32	0.81	1709.18	0.0357	0.85	0.58	0.01	1.07	0.38	Pale yellow	0.04	195	216
539-1-2	1.22	4,833.50	4.73	0.48	3.84	1.56	0.44	0.74	1917.78	0.0513	0.61	0.19	0.03	0.27	-	Pale yellow	△	△	△
539-1-3	0.84	4,140.11	3.71	0.00	14.13	8.56	0.98	1.29	1,321.22	0.3421	1.76	0.23	0.01	0.59	2.00	Pale yellow	0.81	148	180
539-1-4	1.08	4,292.11	4.64	0.00	43.42	13.34	0.76	0.83	1,307.34	1.9937	1.28	0.23	0.00	0.87	14.70	Pale yellow	1.10	130	166
539-1-5	2.23	30,573.28	0.70	0.00	666.01	124.11	6.61	44.69	967.87	5.2021	1.42	223.65	1.08	94.65	152.68	Pale brown	1.78	88	134
540-1-1	5.15	39,249.82	5.53	0.00	617.52	2.58	73.83	87.26	4,462.03	0.0177	0.56	288.28	0.04	58.16	155.07	Pale brown	1.38	113	153
540-1-2	5.98	43,118.06	5.31	0.30	547.26	1.37	60.81	72.21	4,565.55	0.0115	0.66	214.32	0.12	61.51	168.29	Pale brown	1.28	119	158
540-1-3	6.55	47,240.22	5.37	0.20	131.15	0.57	10.01	16.50	5,118.48	0.0083	0.50	33.65	0.03	14.80	55.04	Pale brown	0.85	146	178
540-1-4	5.99	42,463.97	6.72	0.05	198.02	0.05	8.93	11.59	4,155.97	-	0.44	35.94	0.02	13.52	90.89	Pale brown	△	△	△
541-1-1	7.24	47,020.86	4.98	0.18	123.12	1.58	6.25	15.71	8,584.32	-	0.60	41.11	0.01	23.88	9.27	Pale brown	△	△	△
541-1-2	5.23	41,255.09	4.52	0.36	647.07	19.23	81.42	104.58	6,655.28	0.0099	0.61	298.68	0.04	62.24	109.08	Pale brown	1.81	87	133
541-1-3	1.83	3,667.04	2.83	0.00	80.87	18.90	1.46	9.63	1,470.49	1.0427	10.52	5.57	0.00	7.33	24.55	Pale brown	1.26	120	159
541-1-4	0.28	3,846.94	3.12	0.00	85.22	25.58	3.45	7.44	1,410.96	2.6854	16.96	9.07	0.01	1.39	17.84	Pale yellow	1.53	104	146
541-1-5	1.05	3,489.08	1.26	0.00	29.39	7.04	1.69	9.81	1,664.16	0.1330	4.65	3.17	0.01	13.74	4.05	Pale yellow	0.99	137	171
541-1-6	0.96	3,588.26	2.39	1.19	29.26	11.14	1.20	6.78	1,465.37	0.4707	6.46	1.00	0.01	5.95	3.02	Pale yellow	0.90	142	176
540-1-5	2.34	7,216.56	0.48	0.97	226.95	53.94	24.59	16.49	1932.76	0.3145	27.07	76.27	0.01	4.61	42.65	Pale brown	1.67	95	139
540-1-6	1.82	4,688.77	2.89	6.95	132.47	30.79	39.53	13.20	1801.72	0.0961	7.48	49.79	0.04	6.07	24.15	Pale yellow	1.62	98	142
540-1-7	5.45	19,355.93	1.60	0.33	150.30	48.26	0.00	17.34	3,523.68	0.1997	0.67	33.94	0.02	13.20	45.97	Pale brown	1.51	105	147
540-1-8	4.80	13,452.30	0.87	0.90	258.68	93.81	14.56	22.41	2,789.04	0.1718	0.97	68.11	0.06	12.87	64.26	Pale brown	1.78	88	134

Note: -Below the detection limit; △PC1 and homogenization temperature range cannot be calculated because some elements are lower than the detection limit.

yellow part, exceptional enrichment of Pb exists at some positions. It shows that Pb exists mainly in sphalerite in the form of isomorphism ( $Pb^{2+} \leftrightarrow Zn^{2+}$ ) and locally in microinclusions of galena.

Based on the strong correlation between Cu+Ag and Ga+As+Sb (correlation coefficient  $R = 0.712$ ) and in combination with the main valence state of these elements in sulfide and the physical and chemical conditions for ore-forming of the Daliangzi Pb-Zn deposit, we can infer that a possible enrichment mechanism of Ga, As, Ag, Sb, and Cu in sphalerite are  $(Cu+Ag)^{1+} + (Ga+As+Sb)^{3+} \leftrightarrow 2Zn^{2+}$ .

## Indication of trace elements in sphalerite to ore-forming temperature

The composition of trace elements in sphalerite is controlled by temperature and can effectively indicate the ore-forming temperature. Previous studies have shown that Fe, Mn, In, Se, and Te are enriched in sphalerite under high-temperature conditions (e.g., Yunnan Lancang Laochang Pb-Zn deposit) while Ge, Ga, and Cd are relatively enriched in sphalerite under mid-low temperature conditions (e.g., Tianbaoshan Pb-Zn deposit, Niujiaotang Pb-Zn deposit) (Liu et al., 1984; Han

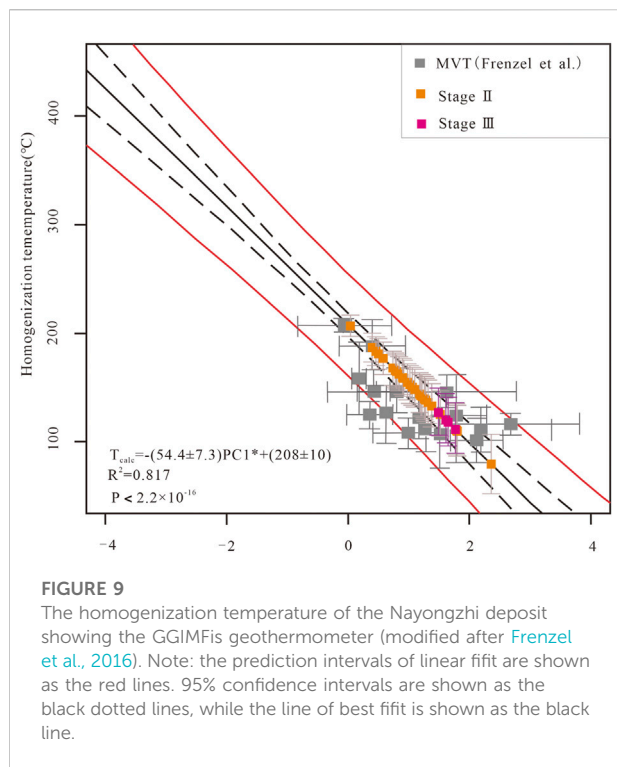


**FIGURE 9**  
The homogenization temperature of the Nayongzhi deposit showing the GGIMFis geothermometer (modified after Frenzel et al., 2016). Note: the prediction intervals of linear fit are shown as the red lines. 95% confidence intervals are shown as the black dotted lines, while the line of best fit is shown as the black line.

et al., 1994; Ye et al., 2011; Ye et al., 2012). The sphalerite of the Daliangzi Pb-Zn deposit is rich in Ge, Ga, and Cd and poor in In and Mn, indicating mid-low temperature ore-forming. The Ga/In the ratio of sphalerite can indicate its formation temperature (Han et al., 1994): in general, Ga/In ratios of 0.001–0.05, 0.01–5, and 1–100 indicate sphalerite under high-, mid-, and low-temperature conditions, respectively. The Ga/In the ratio of the deposit falls within 2.55–1936.29 (253.32 on average), indicating that the sphalerite therein forms under mid-low temperature conditions. Through statistical analysis of trace elements of sphalerite in different types of Pb-Zn deposits

(Frenzel, 2016), believed that the activities of Fe, Ga, Ge, In, and Mn are controlled by ore-forming temperature, and the results the of principal component analysis show a significant correlation between the first principal component (PC1\*) and the ore-forming fluid inclusion ( $R^2=0.82, p<2\times 10^{-16}$ ), which can be expressed by:

$$PC1^* = \ln\left(\frac{C_{Ga}^{0.22} \cdot C_{Ge}^{0.22}}{C_{Fe}^{0.37} \cdot C_{Mn}^{0.20} C_{In}^{0.11}}\right),$$

where Ga, Ge, In, and Mn contents are in ppm while Fe content is in wt%. Based on the correlation, a novel (statistical) sphalerite geothermometer (GGIMFis) is proposed. The relationship between the first principal component (PC1\*) and the homogenization temperature of fluid inclusion (T) is  $T(^{\circ}C) = -(54.4 \pm 7.3) \cdot PC1^* + (208 \pm 10)$ .

The formation temperature of the sphalerite of the deposit estimated by the GGIMFis geothermometer, as shown in Table 1 and Figure 9, is 86–213°C (138°C on average) ~ 133–238°C (173°C on average) (anomaly points deducted), consistent with the temperature measurements in stages II and III of fluid inclusions of the sphalerite of the deposit (118–228°C) (Wang et al., 2018). At one anomaly point probably attributed to low Mn content, the temperature range estimated by GGIMFis is 51–106°C, consistent with the measurement at the point of Mn element anomaly in the mapping diagram (Figure 8). With this anomaly point deducted, the formation temperature of sphalerite in stage II and that in stage III are 86–213°C (138°C on average) ~ 133–238°C (173°C on average) and 88–105°C (96°C on average) ~ 134–147°C (140°C on average), respectively, basically consistent with the temperature measurements of sphalerite and gangue mineral inclusions in stages II and III (Table 3) (Wang et al., 2018), while the formation temperature of sphalerite in stage I is 225.1–320.3°C (264.3°C on average) (Wang et al., 2018), indicating that ore-forming temperature decreases from stage I to stage III of the mineralization period.

**TABLE 2** Contents of trace elements in rocks of different strata in the Sichuan - Yunnan - Guizhou metallogenic domain.

Lithology	Element content(ppm)						
	Pb	Zn	Cu	Co	Cd	Ge	Ag
Emeishan basalt	130.49	414.46	267.14	4.05	0.77	0.63	0.388
Limestone of Qixia- Maokou formation	49.11	108.49	22.44	1.94	2.97	0.23	0.306
Limestone of Weining formation	26.86	80.49	8.08	1.98	0.69	0.64	0.545
Dolostone of Baizuo formation	47.43	120.75	20.69	1.34	2.43	1.13	1.083
Limestone of Datang formation	57.43	135.87	132.93	3.13	2.08	0.74	0.963
Dolostone of Zaige formation	46.23	121.46	7.38	1.91	1.26	0.76	0.488
Dolostone of Dengying formation	64.76	205.48	18.11	2.04	0.299	0.13	0.14
Carbonate in the crust	9	20	4	0.1	0.035	0.2	0.0n

Note: The data on trace element content of carbonate rocks in the crust are quoted from turekian and wedepohl, 1961; Other data are quoted from Han et al., 2006.

TABLE 3 Geological characteristics of the carbonate-hosted non-magmatic epigenetic hydrothermal type lead-zinc deposits in Sichuan–Yunnan–Guizhou metallogenic domain.

Deposit	Position	Hosting strata	Sampling position	Ore-controlling structure	Ore texture	Ore-forming fluids	Source of Ore-forming fluids and materials	References(s)
Huize	NY	Zaige Fm, Baizuo Fm, Dengying Fm	Zaige Fm, Baizuo Fm	The NE direction thrust fold controls the deposit, and the secondary compressional torsional fault or interlayer fault controls the ore body	Massive	Th:150~221°C, 320~364°C; Salinity: 12.0~18.0%, 5.0~11.0%, 1.1~5.0%; log $f_{O_2}$ : 51.5~-37.1	Fluids: basin brine, atmospheric precipitation, and deep fluid	<a href="#">Huang et al., 2004</a> ; <a href="#">Han et al., 2012</a> ; <a href="#">Zhang et al., 2016</a> ; <a href="#">Cui et al., 2017</a> ; <a href="#">Wang et al., 2018</a>
Maoping	NY	Zaige Fm, Baizuo Fm, Weining Fm	Zaige Fm, Baizuo Fm, Weining Fm	NE direction compressional torsional fault and Maomaoshan inverted anticline control the deposit and ore body	Massive, disseminated	Th:200~215°C, 260~300°C; Salinity: 0.8~19.2%	Materials: basement and host rock; Fluids: Basin brine, formation water	<a href="#">Qiu et al., 2013</a> ; <a href="#">Chen, 2014</a> ; <a href="#">Han et al., 2014</a> ; <a href="#">Tan et al., 2019</a>
Huodehong	NY	Qujing Fm	Qujing Fm	NNW direction tensile fault and the southeast wing of Zhaolu anticline	Massive, disseminated, brecciated	Th:80.4~175.6°C	Materials: host rock, underlying strata, a small amount of magmatic material	<a href="#">Jin et al., 2016a</a> ; <a href="#">Wu et al., 2016</a> ; <a href="#">Li et al., 2017</a> ; <a href="#">Chen et al., 2017</a> ; <a href="#">Hu et al., 2021</a>
Lehong	NY	Dengying Fm	Dengying Fm	NW direction tension torsion-tension fracture	Massive, brecciated	Th:Stage I 217.8~310.1°C, Stage II 180.2~241.3°C, Stage III 140.4~227.4°C; Salinity:Stage I 8.81~16.71%, Stage II 7.73~18.47%, Stage III 0.35~19.21%	Materials: basement and sedimentary cover	<a href="#">Zhang et al., 2014</a> ; <a href="#">Cui et al., 2015</a> ; <a href="#">Zhao et al., 2018</a>
Niujiaotang	NG	Qingxudong Fm	Qingxudong Fm	NE direction fault and secondary fault	Brecciated, massive, vein	Th:110~170°C; PH: 6.40~7.30	Materials: wuxun formation; Source of sulfur: seawater sulfate and oilfield brine	<a href="#">Ye et al., 2000</a> , <a href="#">2005</a> , <a href="#">2011</a> ; <a href="#">Jin et al., 2014</a>
Nayongzhi	NG	Qingxudong Fm	Qingxudong Fm	NW direction tensile fault, NE direction anticline, and secondary fault	Banded, stockwork, disseminated	Th:113~232; Salinity: 0.8~15.17%	Materials: basement and host rock; Source of sulfur: Evaporating gypsum	<a href="#">Zhu et al., 2016</a> ; <a href="#">Jin et al., 2016b</a> ; <a href="#">Chen et al., 2017</a> ; <a href="#">Wei et al., 2018</a> ; <a href="#">Yang et al., 2018b</a>
Tianqiao	NG	Huanglong Fm, Baizuo Fm, Datang Fm, Rongxian Fm	Huanglong Fm, Baizuo Fm, Datang Fm	NW direction overpass anticline, controlled by F37 fault	Massive, disseminated, brecciated	Th:150~200°C	Different age strata	<a href="#">Zhou et al., 2015</a> ; <a href="#">Li et al., 2008</a> ; <a href="#">Li, 2016</a>
Tianbaoshan	SS	Dengying Fm	Dengying Fm		Brecciated, massive			

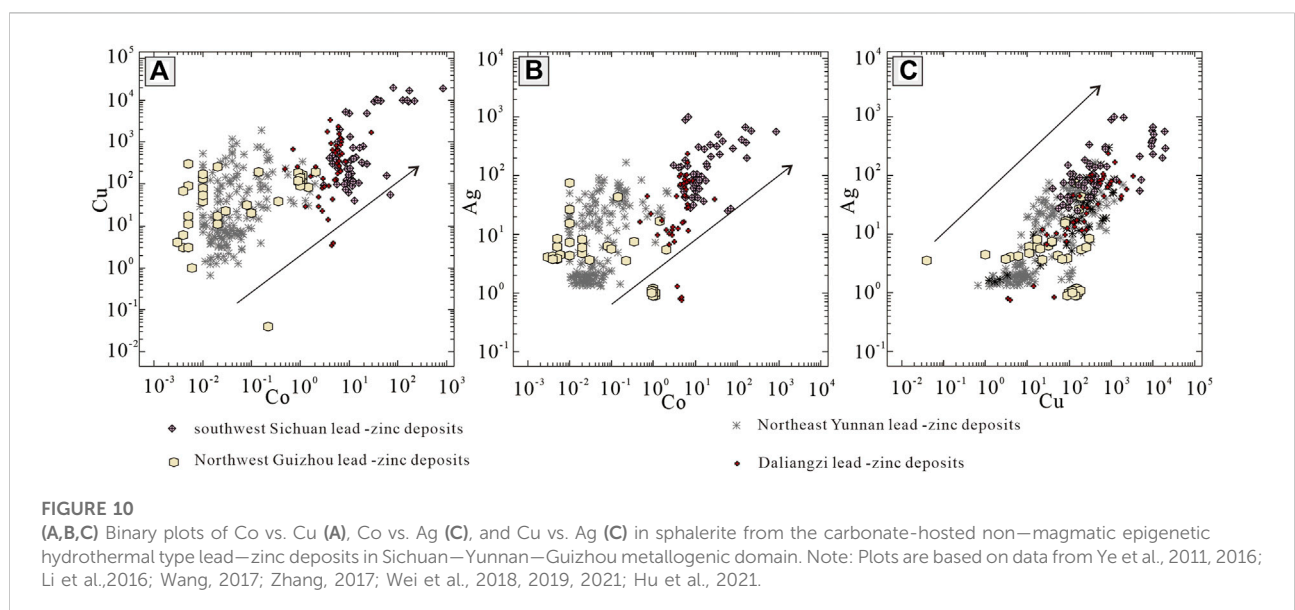
(Continued on following page)

TABLE 3 (Continued) Geological characteristics of the carbonate-hosted non-magmatic epigenetic hydrothermal type lead-zinc deposits in Sichuan-Yunnan-Guizhou metallogenic domain.

Deposit	Position	Hosting strata	Sampling position	Ore-controlling structure	Ore texture	Ore-forming fluids	Source of Ore-forming fluids and materials	References(s)
				EW direction torsional tensile fault controls ore body		Th:Stage II 101.8~267.0°C; Stage III 95.6~158.3°C; Salinity: Stage II 3.2~19.9%; Stage III 2.1~19.9%	Materials: host rock and basement; Fluids: basin brine, atmospheric precipitation, metamorphic water, and organic matter; Source of sulfur: Dengying Formation sulfate and deep source	Zhou et al., 2010; Sun et al., 2016; Ye et al., 2016; Zhang, 2017; Yang et al., 2018a; Wang et al., 2018

As the color of sphalerite becomes lighter (brownish dark—pale brown—pale yellow), Fe content decreases gradually (Table 1). As mentioned above, Fe substitutes Zn in sphalerite in the form of isomorphism ( $Fe^{2+} \leftrightarrow Zn^{2+}$ ); that is to say, Fe exists in sphalerite in the form of FeS. FeS content, however, has a certain relation with the formation temperature of sphalerite and can play the role of a geothermometer (Wang et al., 1982). In general, the sphalerite of high-mid temperature deposit contains 12.24~15.9% FeS, with a formation temperature of 400~500°C, while that of the mesothermal deposit contains 4.63~7.74% FeS, with formation temperature of 100~200°C. The

formation temperature should have decreased gradually as the color of sphalerite becomes lighter and Fe content decreases gradually, but the formation temperature of sphalerite estimated by GGIMFis geothermometer is just the other way round (e.g., 539# sample)—higher Fe content corresponds to lower formation temperature, which may be caused by nonuniform distribution of trace elements (existence of extreme point) or relatively narrow sphalerite band (denudation). Nevertheless, both the formation temperature estimated by the GGIMFis geothermometer and that by the FeS geothermometer fall within the low-mid temperature range.



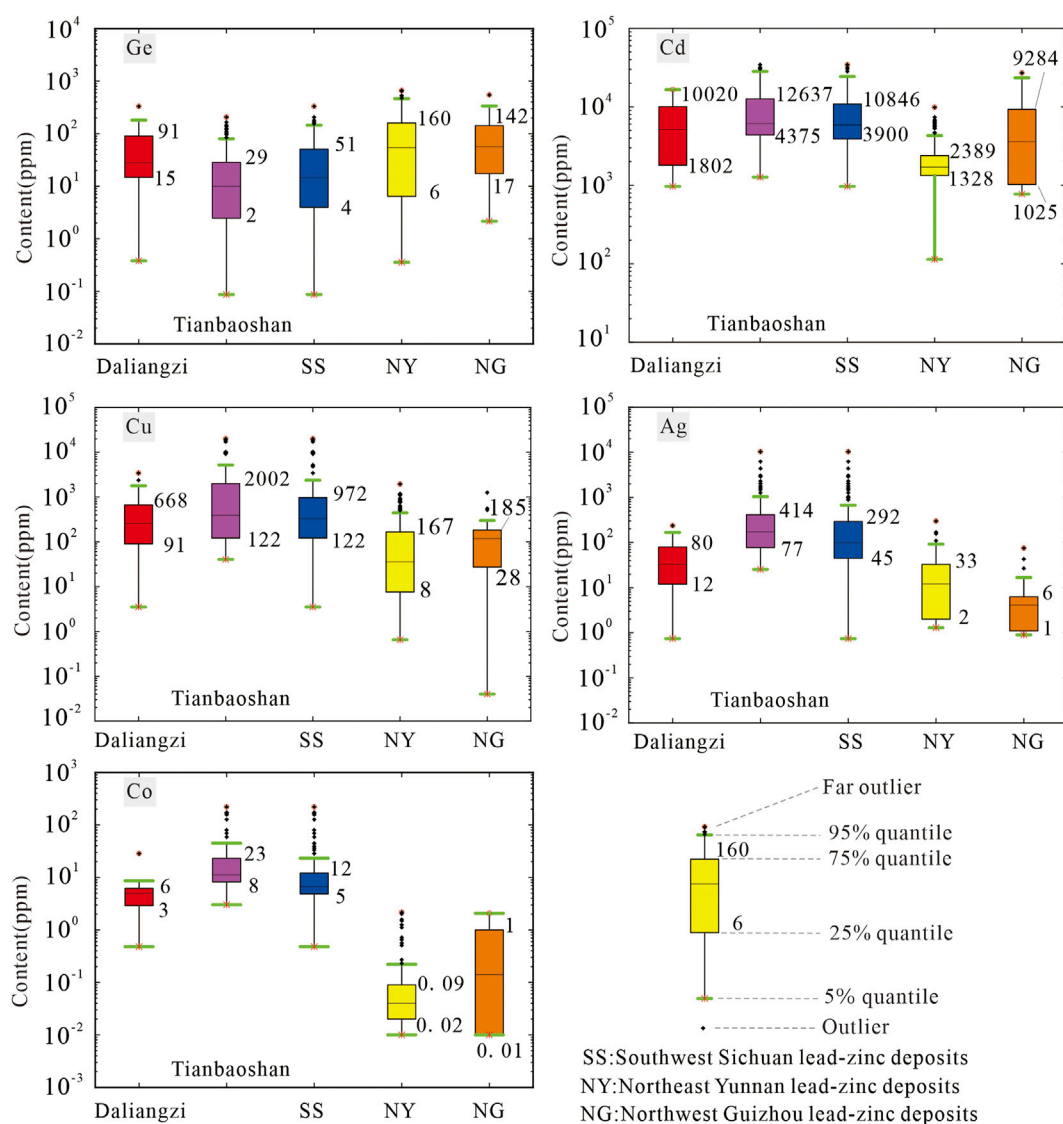


**FIGURE 11**

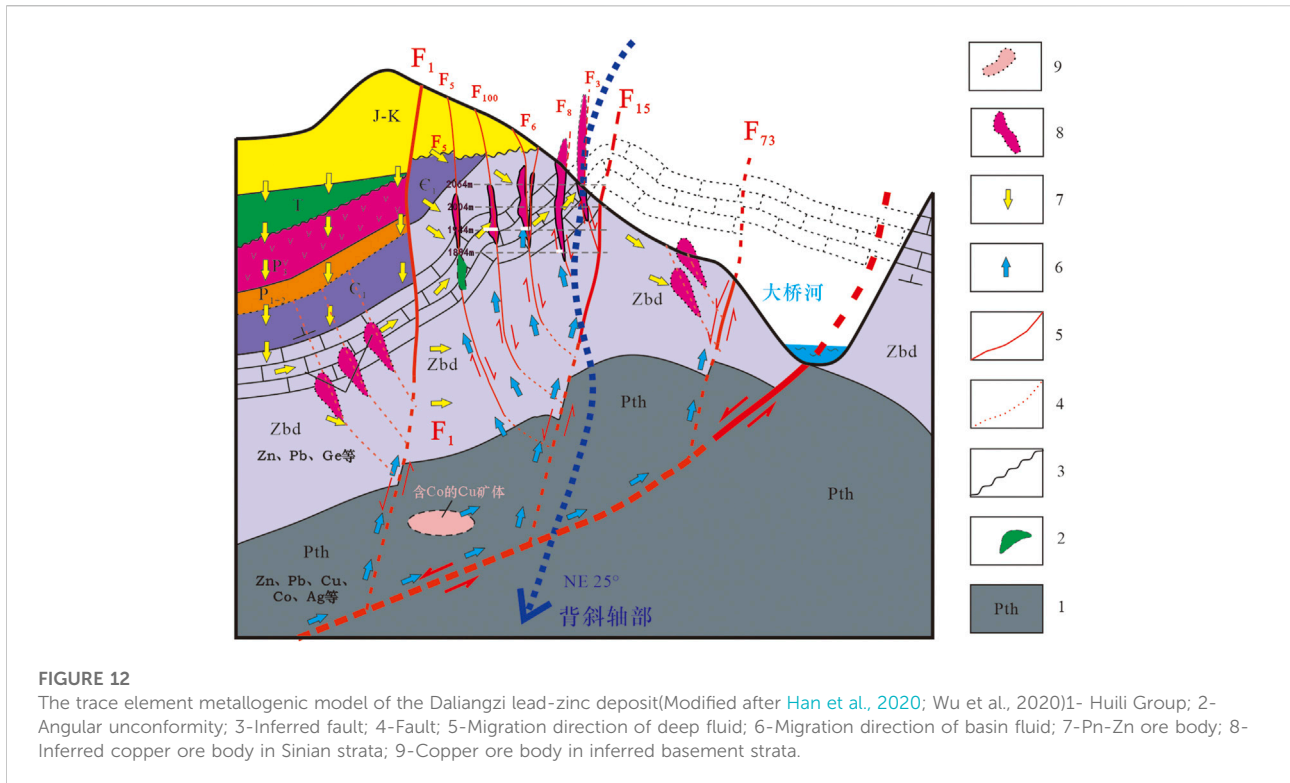
Box-and-whisker plots of the trace element results of sphalerite from the carbonate-hosted non-magmatic epigenetic hydrothermal type lead-zinc deposits in Sichuan-Yunnan-Guizhou metallogenic domain. Note: Plots are based on data from Ye et al., 2011, 2016; Li et al., 2016; Wang, 2017; Zhang, 2017; Wei et al., 2018, 2019, 2021; Hu et al., 2021.

To sum up, the Daliangzi Pb-Zn deposit should be magmatic epigenetic hydrothermal Pb-Zn deposit hosted by carbonate forming under mid-low temperature conditions.

## Implications of trace element signatures of sphalerite for deep prospecting of deposit

Through LA-ICP-MS measurement of trace elements of the sphalerite of Daliangzi Ge-enriched Pb-Zn deposit and comprehensive comparative study based on trace element

data of the sphalerite in 3 ore-concentrated areas, i.e., northeast Yunnan, northwest Guizhou, and southwest Sichuan, it is found that the sphalerite of Pb-Zn deposit in the ore-concentrated area of southwest Sichuan is richer than that in northeast Yunnan and northwest Guizhou in Co (213.66 and 60.70 times, respectively), Cu (12.65 and 12.53 times, respectively), and Ag (6.11 and 17.76 times, respectively), but poorer in Ge (0.38 and 0.44 times, respectively) (Figure 11). The differences in trace elements of sphalerite in different ore-concentrated areas may be related to physical and chemical conditions for ore forming (e.g., temperature,  $f_{O_2}$ , and PH), material source, water-rock



reaction, etc. (Bethke et al., 1971; Scott et al., 1971; Barton et al., 1977; Cook et al., 2009).

Most of the deposits in southwest Sichuan, northeast Yunnan, and northwest Guizhou ore-concentrated areas have formed under the weak acid-weak base and weak reduction-weak oxidation conditions, of which Huize Pb-Zn deposit in northeast Yunnan ore-concentrated area has formed under acid conditions in stage I (Zhang, 2016), but the trace elements of sphalerite thereof are close to those of sphalerite of Maoping Pb-Zn deposit in northeast Yunnan ore-concentrated area. Most scholars believe that Ge enrichment is closely related to mid-low temperature ore-forming fluid (Bellissont et al., 2014; Cugerone et al., 2018); Huize Pb-Zn deposit in northeast Yunnan ore-concentrated area is mostly mid and high-temperature, but Ge content thereof (65.90 ppm on average) is basically consistent with that of Maoping Pb-Zn deposit (46.17 ppm on average), which is mostly low-temperature (Ye et al., 2011; Wang et al., 2017; Wei et al., 2021), while Huodehong Pb-Zn deposit (Ge content of 168.27 ppm on average) and Lehong Pb-Zn deposit (Ge content of 133.82 ppm on average), for which the ore-forming temperature is close to that of Maoping Pb-Zn deposit, are obviously rich in Ge. It follows that the physical and chemical conditions (temperature,  $f_{O_2}$ , PH, etc.) for ore-forming in different ore-concentrated areas have limited influence on the degree of enrichment of trace elements of sphalerite.

During the research of the Maoping Pb-Zn deposit (Wei et al., 2021), noticed that water-rock reaction has been commonly developed and speculated that host rock has a certain influence upon the trace element content of sphalerite, but the contents of trace elements (e.g., Cu, Co, Ag, and Ge) of sphalerite in Carboniferous-Devonian carbonate formation of northeastern Yunnan and northwestern Guizhou ore-concentrated areas are close; the trace elements of sphalerite in southwestern Sichuan ore-concentrated area, where ore bodies mainly occur in the Sinian Dengying Formation, are obviously different from those of sphalerite in northeastern Yunnan and northwestern Guizhou ore-concentrated areas, but there is no significant difference between the trace element contents in dolomite of Dengying Formation and those in dolomite of Zaige Formation and Baizuo Formation (Table 2). It follows that host rock also has a limited influence upon trace element contents of sphalerite. Considering that the ore-forming fluid in the ore-forming area is characterized by sedimentary mineralization after mixing of deep source fluid (migration of Pb and Zn in the form of chloride complex) and basin fluid (Zhang, 2016) (Table 3), it can be inferred that basement strata are likely to play an important role in enrichment of trace elements of sphalerite.

Co-bearing Cu deposits are commonly developed in basement strata, such as the Yimen Shizishan Cu deposit (Ji, 2009) and Huidong Youfanggou Cu deposit (Jiang et al., 2015),

and Cu has a high background value (Shen et al., 2006), providing a good material base for enrichment of Cu, Co, and Ag (Du et al., 2019); find during the study of the geochemical background of the western margin of Yangtze plate that Ge is mainly enriched in basement strata. Studies show that there is a good positive correlation between Co and Cu/Ag and between Cu and Ag (Figure 10), indicating that Pb-Zn formation may be related to basement strata. Ore-forming fluid extracts such trace elements as Cu, Co, Ge, and Ag of basement strata, migrates in the form of chloride complex driven by tectonic dynamic, and mixes with basin fluid in the stratum of carbonatite of Sinian Dengying Formation, causing the precipitation of metallic minerals and thus the formation of Pb-Zn ore body; if the fluid extracts sufficient Cu, concealed Cu ore body may exist at depth of Pb-Zn ore body (Sun et al., 2016). This may be the reason why the sphalerite of Pb-Zn deposit in the southwest Sichuan ore-concentrate area is richer in Co, Cu, and Ag (Figure 11) but poorer in Ge (Figure 11) than that in northeast Yunnan and northwest Guizhou ore-concentrated areas, indicating that the enrichment of Co, Cu, and Ag probably restrains that of Ge, which is consistent with the result discussed earlier that Cu (Ag) and Ge substitute Zn by coupling in sphalerite. Ore-forming fluid constantly migrates to the top and extracts trace elements flowing through stratum and host rocks, and then mixes with basin fluid in the stratum of carbonatite of Sinian Dengying Formation, causing the precipitation of metallic minerals and thus the formation of Pb-Zn ore body, but Cu, Co, and Ag contents in ore-forming fluid decrease while Ge content increases correspondingly, leading to relative enrichment of Ge and loss of Cu, Co, and Ag (Figure 11) in sphalerite of Pb-Zn deposit in northeast Yunnan and northwest Guizhou ore-concentrated areas. Meanwhile, we notice that no obvious difference in Cd content can be seen in these three ore-concentrated areas, which may be related to the enrichment of Cd in both basement and ore-host strata (Du et al., 2019).

To sum up, the ore-forming model of the Daliangzi Ge-rich Pb-Zn deposit (Figure 12) indicates that the favorable position of structure in the Sinian Dengying Formation outside of the ore-forming area is the key direction for finding Pb-Zn ores and that of the deep Sinian carbonate formation and structure inside Sichuan-Yunnan-Guizhou ore-forming areas has the potential for finding Pb-Zn (or Cu) ore bodies, and concealed Cu ore bodies may also exist at depth.

## Conclusion

1) Sphalerite is characterized by rich Cd, Ge, and Ga, relatively rich Fe, very variable Cu and Pb contents, and poor Mn, In, and Sn; the good correlation between Cu (Ag) and Ge and that between (Cu+Ag) and (Ga+As+Sb) suggest that the

substitution relationship with Zn is  $n\text{Cu}^{2+} + \text{Ge}^{2+} \leftrightarrow (n+1)\text{Zn}^{2+}$  or  $n(\text{Cu}, \text{Ag})^{2+} + \text{Ge}^{2+} \leftrightarrow (n+1)\text{Zn}^{2+}$  and  $(\text{Cu} + \text{Ag})^{1+} + (\text{Ga} + \text{As} + \text{Sb})^{3+} \leftrightarrow 2\text{Zn}^{2+}$ , respectively, and chalcopyrite and Ge, Ga, and Ga-rich microinclusions exist locally.

- 2) From stage II to stage III, Ge, Gd, Cu, Pb, Fe, and Mn contents decrease gradually while Ga content increases gradually; Ge, Gd, Cu, Pb, Fe, and Mn contents in the pale brown part are higher than those in the pale-yellow part of banded sphalerite while Ga and In are relatively enriched in pale yellow sphalerite.
- 3) The formation temperature of sphalerite at stage II and that at stage III of hydrothermal mineralization are 51–213°C (136°C on average)–106–238°C (171°C on average) and 88–105°C (96°C on average)–134–147°C (140°C on average), respectively, indicating that temperature drops during the formation of sphalerite in combination with the temperature measurements of sphalerite inclusions. The ore-forming temperature reflects the characteristics of a mid-low deposit, indicating that the deposit is a typical epigenetic Pb-Zn deposit hosted by carbonatite forming under mid-low temperature conditions.
- 4) Based on the established ore-forming model of the Daliangzi Ge-rich Pb-Zn deposit, it is speculated that concealed Cu ore bodies may exist at the depth of the ore-forming area and the favorable position of structure in the Sinian Dengying Formation outside is the key direction for finding Pb-Zn deposits.

## Data availability statement

The original contributions presented in the study are included in the article/Supplementary Material, further inquiries can be directed to the corresponding author.

## Author contributions

Author contributions LL: Conceptualization, Software, Investigation, Experiment, Data Curation, Writing—Original Draft. RH: Validation, Methodology, Investigation, Formal analysis, Visualization, Supervision. YZ: Validation, Formal analysis, Investigation. JW: Validation, Formal analysis, Investigation. ZF: Investigation, Experiment, Writing: Review and Editing.

## Funding

This work was co-financed by the programs of the National Natural Science Foundation (Nos. 42172086, 41572060, and U1133602), the Program of “Yunling Scholar” of Yunnan province (2014), Projects of Yunnan Engineering Laboratory of Mineral Resources Prediction and Evaluation (YM Lab) (2010) and Innovation Team of Yunnan province and KMUST (2008, 2012).

## Conflict of interest

ZF was employed by the company Sichuan Huidong Daliang Mining Co. Ltd.

The remaining authors declare that the research was conducted in the absence of any commercial or financial relationships that could be construed as a potential conflict of interest.

## References

- Barton, P. B., Bethke, P. M., and Roedder, E. (1977). Environment of ore deposition in the Creede mining district, San Juan Mountains, Colorado; Part III, Progress toward interpretation of the chemistry of the ore-forming fluid for the OH Vein. *Econ. Geol.* 72 (1), 1–24. doi:10.2113/gsecongeo.72.1.1
- Belissant, R., Boiron, M. C., Luais, B., and Cathelineau, M. (2014). LA-ICP-MS analyses of minor and trace elements and bulk Ge isotopes in zoned Ge-rich sphalerites from the Noailhac – saint-Salvy deposit (France): Insights into incorporation mechanisms and ore deposition processes. *Geochimica Cosmochimica Acta* 126, 518–540. doi:10.1016/j.gca.2013.10.052
- Belissant, R. (2016). France: Dissertation, Lorraine: Université de Lorraine. Ph. D1-240. Germanium and related elements in sulphide minerals: Crystal chemistry, incorporation and isotope fractionation[D]
- Bethke, P. M., and Barton, P. B. (1971). Distribution of some minor elements between coexisting sulfide minerals. *Econ. Geol.* 66 (1), 140–163. doi:10.2113/gsecongeo.66.1.140
- Bonnet, J., Mosser-Ruck, R., Caumon, M. C., Rouer, O., Andre-Mayer, A. S., Cauzid, J., et al. (2016). Trace element distribution (Cu, Ga, Ge, Cd, and Fe) in sphalerite from the Tennessee MVT deposits, USA, by combined EMPA, LA-ICP-MS, Raman spectroscopy, and crystallography. *Can. Mineral.* 54 (5), 1261–1284. doi:10.3749/canmin.1500104
- Chen, Q. L. (2017). Prospecting progress of lead-zinc (silver) deposits in Zhaotong area, Yunnan and comparison of typical deposits[J]. *Nonferrous Met. Min. Sect.* 69 (6), 39–46. (in Chinese). doi:10.39/j.issn.1671-4172.2017.06.010
- Chen, S. H. (2014). *Altered lithofacies research and tectonic geochemical prospecting prediction of Zhaotong lead-zinc deposit in Yunnan[D]*. China: Kunming University of Science and Technology. (in Chinese). doi:10.3969/j.issn.0001-5717.2017.06.008
- Chen, W., Kong, Z. G., Liu, F. X., et al. (2017). Geology, geochemistry and Genesis of the Nayongzhi lead-zinc deposit in Guizhou[J]. *Acta Geol.* 91 (6), 1269–1284. (in Chinese).
- Cook, N. J., Ciobanu, C. L., Pring, A., Skinner, W., Shimizu, M., Danyushevsky, L., et al. (2009). Trace and minor elements in sphalerite: A LA-ICPMS study. *Geochimica Cosmochimica Acta* 73 (16), 4761–4791. doi:10.1016/j.gca.2009.05.045
- Cook, N. J., Etschmann, B., Ciobanu, C. L., Geraki, K., Howard, D., Williams, T., et al. (2015). Distribution and substitution mechanism of Ge in a Ge-(Fe)-bearing sphalerite. *Minerals* 5 (2), 117–132. doi:10.3390/min5020117
- Cugerone, A., Cenki-Tok, B., Chauvet, A., Le Goff, E., Bailly, L., Alard, O., et al. (2018). Relationships between the occurrence of accessory Ge-minerals and sphalerite in Variscan Pb-Zn deposits of the Bossost anticlinorium, French Pyrenean Axial Zone: Chemistry, microstructures and ore-deposit setting. *Ore Geol. Rev.* 95, 1–19. doi:10.1016/j.oregeorev.2018.02.016
- Cui, J. H., Han, R. S., and Zhao, D. (2015). Analysis of the metallogenic structure system in the Lehong lead-zinc ore area in northeastern Yunnan[J]. *Acta Mineral. Sin.* (S1), 994–995. (in Chinese). doi:10.16461/j.cnki.1000-4734.2015.s1.718
- Cui, Y. L., Zhou, J. X., Huang, Z. L., and Luo, K. (2017). Geology, geochemistry and Genesis of the Fule lead-zinc deposit in Yunnan[J]. *Acta Petrol. Sin.* 34 (1), 194–206. (in Chinese).
- Cui, Z. L., Liu, X. Y., He, S., and Kong, D. K. (2018). Discussion on ore-forming materials and fluid sources in huize super large lead-zinc ore field—H, O, S, C isotopic geochemical evidence[J]. *J. Hebei Univ. Geosciences* 41 (1), 45–52. (in Chinese). doi:10.13937/j.cnki.hbdzdx.2018.01.003
- Du, S. J., Wen, H. J., Zhu, C. W., Luo, Z. G., Zhou, Z. B., Yang, Z. M., et al. (2019). Geochemical background of supernormal enrichment of rare metals in the Western margin of Yangtze Plate[J]. *Acta Petrol. Sin.* 35 (11), 3355–3369. (in Chinese). doi:10.18654/1000-0569/2019.11.06
- Frenzel, M., Hirsch, T., and Gutzmer, J. (2016). Gallium, germanium, indium, and other trace and minor elements in sphalerite as a function of deposit type — a meta-analysis. *Ore Geol. Rev.* 76, 52–78. doi:10.1016/j.oregeorev.2015.12.017
- George, L., Cook, N. J., Ciobanu, C. L., and Wade, B. P. (2015). Trace and minor elements in galena: A reconnaissance LA-ICP-MS study. *Am. Mineralogist* 100 (2–3), 548–569. doi:10.2138/am-2015-4862
- George, L., Cook, N. J., and Ciobanu, C. L. (2016). Partitioning of trace elements in co-crystallized sphalerite-galena-chalcopryrite hydrothermal ores. *Ore Geol. Rev.* 77, 97–116. doi:10.1016/j.oregeorev.2016.02.009
- Han, R. S., Chen, J., Huang, Z. L., Ma, D. Y., Xue, C. D., Li, Y., et al. (2006). *Tectonic mineralization dynamics and concealed deposit location prediction: A case study of the super-large lead-zinc (silver, germanium) deposit in huize*. Yunnan: Springer. (in Chinese).
- Han, R. S., Hu, Y. Z., Wang, X. K., Huang, Z. L., Chen, J., Wang, F., et al. (2012). Deposit model of germanium-rich silver-lead-zinc polymetallic ore concentration area in northeastern Yunnan[J]. *Acta Geol.* 86 (2), 280–294. (in Chinese). doi:10.3969/j.issn.0001-5717.2012.02.007
- Han, R. S., Liu, C. Q., Huang, Z. L., Chen, J., Ma, D. Y., Lei, L., et al. (2007b). Geological features and origin of the huize carbonate-hosted Zn-Pb-(Ag) district, yunnan, south China. *Ore Geol. Rev.* 31 (1–4), 360–383. doi:10.1016/j.oregeorev.2006.03.003
- Han, R. S., Wang, F., Hu, Y. Z., and Wang, X. (2014). Metallogenic structure dynamics and chronological constraints of the Huize-type (HZZT) germanium-rich silver-lead-zinc deposit[J]. *Tect. Mineralogy* 38 (4), 758–771. (in Chinese). doi:10.16539/j.ddgzyckx.2014.04.003
- Han, R. S., Wu, P., Zhang, Y., Huang, Z. L., Wang, F., Jin, Z. G., et al. (2021). New research progresses of metallogenic theory for Zn-Pb-(Ag-Ge) deposits in the sichuan-yunnan-guizhou triangle (SYGT) area, southwestern tethys. *Acta. Geol. Sin.*, 95. (in Chinese) <http://www.geojournals.cn/dzxb/ch/index.aspx>.
- Han, R. S., Zhang, Y., Ren, T., Qiu, W. L., Wei, P. T., et al. (2020). A summary of research on carbonate-hosted, non-magmatic, epigenetic, hydrothermal type Pb-Zn deposits[J]. *J. Kunming Univ. Sci. Technol. Natural Sci.* 45 (04), 29–40. (in Chinese). doi:10.16112/j.cnki.53-1223/n.2020.04.005
- Han, Z. X. (1994). The typomorphic characteristic of the sphalerite in the QingLing devonian system lead-zinc metallogenic belt [J]. *J. Xi'an Eng. Univ.* 16 (1), 12–17. (in Chinese).
- Hu, R. Z., Fu, S. L., Huang, Y., Zhou, M. F., Fu, S. H., Zhao, C., et al. (2017a). The giant South China Mesozoic low-temperature metallogenic domain: Reviews and a new geodynamic model. *J. Asian Earth Sci.* 137, 9–34. doi:10.1016/j.jseas.2016.10.016
- Hu, Y. S., Ye, L., Huang, Z. L., et al. (2019). Distribution and existing forms of trace elements from maliping Pb-Zn deposit in northeastern yunnan, China: A LA-ICPMS study[J]. *Acta Petrol. Sin.* 35 (11), 3477–3492. doi:10.18654/1000-0569/2019.11.14
- Hu, Y., Wei, C., Ye, L., Huang, Z., Danyushevsky, L., and Wang, H. (2021). LA-ICP-MS sphalerite and galena trace element chemistry and mineralization-style fingerprinting for carbonate-hosted Pb-Zn deposits: Perspective from Early Devonian Huodehong deposit in Yunnan, South China[J]. *Ore Geol. Rev.* 136, 104253. doi:10.1016/j.oregeorev.2021.104253
- Hu, Z., Zhang, W., Liu, Y., Gao, S., Li, M., Zong, K., et al. (2015). “Wave” signal-smoothing and mercury-removing device for laser ablation quadrupole and multiple collector ICPMS analysis: Application to lead isotope analysis. *Anal. Chem.* 87 (2), 1152–1157. doi:10.1021/ac503749k

## Publisher's note

All claims expressed in this article are solely those of the authors and do not necessarily represent those of their affiliated organizations, or those of the publisher, the editors, and the reviewers. Any product that may be evaluated in this article, or claim that may be made by its manufacturer, is not guaranteed or endorsed by the publisher.

- Huang, Z. L., Chen, J., Han, R. S., and Li, W. B. (2004). Geochemistry and Genesis of the Huize super-large lead-zinc deposit in yunnan: A discussion on the relationship between emeishan basalt and lead-zinc mineralization[J]. *Geol. Publ. House* 29 (48), 68–72. Beijing.
- Ishihara, S., Hoshino, K., Murakami, H., and Endo, Y. (2006). Resource evaluation and some genetic aspects of indium in the Japanese ore deposits. *Resour. Geol.* 56 (3), 347–364. doi:10.1111/j.1751-3928.2006.tb00288.x
- Ji, L. N. (2009). *Research on the geological characteristics of yimen lion mountain copper deposit and the occurrence law of cobalt and silver*[D]. China: Kunming University of Science and Technology. (in Chinese).
- Jiang, X. F., Wang, S. W., Liao, Z. W., Zhou, Q., Guo, Y., Zhou, B. G., et al. (2015). Re-Os isotopic age of Youfanggou copper deposit in Huidong, Sichuan and its geological significance[J]. *Tect. Mineralogy* 39 (5), 866–875. (in Chinese). doi:10.16539/j.ddgzyckx.2015.05.010
- Jin, C. H., Zhang, Y., Shen, Zh W., and Zhang, D. (2016a). Geological characteristics and ore-forming sources of the huode red lead-zinc deposit in northeastern yunnan[J]. *Mineralogy* 36 (4), 50–56. (in Chinese). doi:10.19719/j.cnki.1001-6872.2016.04.007
- Jin, C. H., Zhang, Y., Zhang, D., Zhao, Z., Huang, L., Tan, H., et al. (2014). Metallogenic model of Niujiaotang lead-zinc deposit in duyun, Guizhou[J]. *Mineral. Deposits* 33 (S1), 699–700. (in Chinese).
- Jin, Z. G. (2008). China: Metallurgical Industry Press. (in Chinese). Lead-zinc deposits in northwestern Guizhou, ore-controlling factors, metallogenic regularities and prospecting predictions[M]
- Jin, Z. G., Zhou, J. X., and Huang, Z. L. (2016b). Genesis of the Nayongzhi lead-zinc deposit in puding, Guizhou: S and *in-situ* Pb isotopic evidence[J]. *Acta Petrol. Sin.* 32 (11), 3441–3455. (in Chinese).
- Keith, M., Haase, K. M., Schwarz-Schampera, U., Klemm, R., Petersen, S., and Bach, W. (2014). Effects of temperature, sulfur, and oxygen fugacity on the composition of sphalerite from submarine hydrothermal vents. *Geology* 42 (8), 699–702. doi:10.1130/g35655.1
- Kong, Z. G., Zhang, B. C., Wu, Y., Zhang, C. Q., Liu, Y., Zhang, F., et al. (2021). Structure controlling pattern and metallogenic mechanism of the Daliangzi germanium-rich Pb-Zn deposit, Sichuan Province, China[J]. *Earth Sci. Front.*, 1–21. (in Chinese). doi:10.13745/j.esf.2021.5.1
- Leach, D. L., and Song, Y. (2019). Sediment-hosted zinc-lead and copper deposits in China: Society of economic geologists[J]. *Spec. Publ.* 22, 325–409. doi:10.5382/SP.22.09
- Li, F. Y. (2003). *Study on the occurrence state and enrichment mechanism of dispersed elements in MVT lead-zinc deposits-taking tianbaoshan and Daliangzi lead-zinc deposits in sichuan as an example: Master's degree thesis*[D]. China: Chengdu University of Technology. (in Chinese).
- Li, Z. L., Ye, L., Hu, Y. S., and Huang, Z. L. (2017). Preliminary study on *in-situ* sulfur isotopes of the Huodehong lead-zinc deposit in northeastern yunnan[J]. *Collect. Abstr. Pap. Eighth Natl. Symposium Mineralization Theory Prospect. Methods*, 135. (in Chinese).
- Li, Z. L., Ye, L., Huang, Z. L., Nian, H. L., and Zhou, J. X. (2016). Preliminary study on trace element composition of sphalerite from Tianqiao lead-zinc deposit in Guizhou[J]. *Acta Mineral. Sin.* 36 (2), 183–188. (in Chinese).
- Li, Z. L. (2016). China: Guiyang: Institute of Geochemistry, Chinese Academy of Sciences. Master's degree thesis. Metallogenic geology and geochemistry and prospecting direction of the Fule lead-zinc deposit in Yunnan[D]
- Liu, H. C., and Lin, W. D. (1999). Kunming: Yunnan University Press, 1–468. (in Chinese). Regularity research of Pb-Zn-Ag ore deposits in northeast yunnan, China[M]
- Liu, Y., Hu, Z., Gao, S., Gunther, D., Xu, J., Gao, C., et al. (2008). *In situ* analysis of major and trace elements of anhydrous minerals by LA-ICP-MS without applying an internal standard. *Chem. Geol.* 257 (1–2), 34–43. doi:10.1016/j.chemgeo.2008.08.004
- Liu, Y. J., Cao, L. M., Li, Z. L., Wang, H. N., Chu, T. Q., Zhang, J. R., et al. (1984). Beijing: Geological Publishing House, 1–548. (in Chinese). Element geochemistry[M]
- Möller, P. (1987). Correlation of homogenization temperatures of accessory minerals from sphalerite-bearing deposits and Ga/Ge model temperatures. *Chem. Geol.* 61 (1–4), 153–159. doi:10.1016/0009-2541(87)90035-0
- Mondillo, N., Arfè, G., Herrington, R., Boni, M., Wilkinson, C., and Mormone, A. (2018). Germanium enrichment in supergene settings: Evidence from the cristall nonsulfide Zn prospect, bongará district, northern Peru. *Min. Depos.* 53 (2), 155–169. doi:10.1007/s00126-017-0781-1
- Paton, C., Hellstrom, J., Paul, B., Woodhead, J., and Hergt, J. (2011). Iolite: Freeware for the visualisation and processing of mass spectrometric data. *J. Anal. At. Spectrom.* 26 (12), 2508–2518. doi:10.1039/c1ja10172b
- Qiu, W. L. (2013). Kunming: Master's Thesis of Kunming University of Science and Technology. (in Chinese). Research on fluid geochemistry of Zhaotong lead-zinc deposit in Yunnan[D]
- Scott, S. D., and Barnes, H. L. (1971). Sphalerite geothermometry and geobarometry. *Econ. Geol.* 66, 653–669.
- Shen, H. M., Li, J. Z., Zhang, W. K., Yi, Z. M., Peng, Z. S., Shi, L. F., et al. (2006). Chengdu: Sichuan Geological Survey Institute. (in Chinese). Report on evaluation results of Huidong copper lead zinc polymetallic deposit in Sichuan
- Sun, H. R., Zhou, J. X., Huang, Z. L., Fan, H. F., Ye, L., Luo, K., et al. (2016). Discussion on the genetic relationship between newly discovered copper deposits and lead-zinc deposits in the deep part of Tianbaoshan deposit in Huili, Sichuan[J]. *Acta Petrol. Sin.* 32 (11), 3407–3417. (in Chinese).
- Tan, S. C., Zhou, J. X., Luo, K., Xiang, Z. Z., He, X. H., Zhang, Y. H., et al. (2019). The source of minerals from the maoping large lead-zinc deposit in yunnan: *In-situ* S and Pb isotopic constraints[J]. *Acta Petrol. Sin.* 35 (11), 3461–3476. (in Chinese).
- Tu, G. Z., Gao, Z. M., and Hu, R. Z. (2003). *Dispersed element Geochemistry and metallogenic mechanism*[M]. Beijing: Geological Publishing House, 1–424. (in Chinese).
- Wang, C. M., Deng, J., Zhang, S. T., Xue, C. J., Yang, L. Q., Wang, Q. F., et al. (2010). Sediment-hosted Pb-Zn deposits in southwest sanjiang tethys and kangdian area on the Western margin of Yangtze craton. *Acta Geol. Sin.* 84 (6), 1428–1438.
- Wang, F., Chen, J., and Luo, D. F. (2013). China: Ke xue chu ban she. (in Chinese). Analysis of lead-zinc mineral resource potential and prospecting law in the bordering area of Sichuan, Yunnan and Guizhou[M]
- Wang, H., Wang, J. B., Zhu, X. Y., Li, Y. S., Zhen, S. M., Sun, H. R., et al. (2018). Genesis of the Daliangzi lead-zinc deposit on the western margin of the Yangtze platform: Fluid inclusions and isotope geochemical constraints[J]. *Tect. Mineralogy* 42 (4), 681–698. (in Chinese).
- Wang, J. (2018). *Research on the positioning law of large lead-zinc deposits in the southwestern margin of the upper and middle Yangtze platform*[D]. Wuhan: China University of Geosciences. (in Chinese).
- Wang, P., Pan, Z. L., and Weng, L. B. (1982). Beijing: Geological Publishing House. (in Chinese). Systematic mineralogy[M]
- Wang, X. C. (1991). Genetic analysis of the Daliangzi lead-zinc deposit in Sichuan [J]. *Mineral. deposits* 22 (3), 151–156. (in Chinese).
- Wang, Z. J., and Wang, A. R. (1985). Sedimentary Genesis of ancient karst caves in the Daliangzi lead-zinc deposit, Tianbaoshan, Sichuan[J]. *Geol. Prospect.* 10, 10–17. (in Chinese).
- Wang, Z. Q. (2017). *Enrichment of dispersed elements in the Huize super large lead-zinc deposit in Yunnan*[D]. Beijing: China University of Geosciences. (in Chinese).
- Wei, C., Huang, Z., Yan, Z., Hu, Y., and Ye, L. (2018a). Trace element contents in sphalerite from the Nayongzhi Zn-Pb deposit, northwestern Guizhou, China: Insights into incorporation mechanisms, metallogenic temperature and ore genesis. *Minerals* 8 (11), 490. doi:10.3390/min8110490
- Wei, C., Yan, Z. F., Huang, Z. L., and Hu, Y. S. (2018b). Geochemical characteristics of hydrothermal dolomite from the Nayongzhi lead-zinc deposit in northwestern Guizhou and its prospecting indications[J]. *Acta Mineral. Sin.* 38 (06), 666–674. (in Chinese).
- Wei, C., Ye, L., Hu, Y., Danyushevskiy, L., Li, Z., and Huang, Z. (2019). Distribution and occurrence of Ge and related trace elements in sphalerite from the Lehong carbonate-hosted Zn-Pb deposit, northeastern Yunnan, China: Insights from SEM and LA-ICP-MS studies. *Ore Geol. Rev.* 115, 103175. doi:10.1016/j.oregeorev.2019.103175
- Wei, C., Ye, L., Hu, Y., Leonid, D., and Haoyu, W. (2021). MS analyses of trace elements in base metal sulfides from carbonate-hosted Zn-Pb deposits, south China: A case study of the maoping deposit[J]. *Ore Geology Reviews*, 130, 103945. doi:10.1016/j.oregeorev.2020.103945LA-ICP-
- Wen, H. J., Zhou, Z. B., Zhu, C. W., Luo, Z. G., Zhu, C. W., Du, S. J., et al. (2019). The main scientific problems of supernormal enrichment of rare metals[J]. *Acta Petrol. Sin.* 35 (11), 3271–3291. (in Chinese).
- Wu, J. B., Han, R. S., Feng, Z. X., Wu, P., Gong, H. S., Ding, T. Z., et al. (2021). F15 main controlling fault and its ore-controlling effect in Daliangzi lead-zinc deposit of southwestern sichuan, China[J]. *Geol. Bull. China* 10, 1–23. [2021-10-9] <http://kns.cnki.net/kcms/detail/11.4648.P.20210421.1319.002.html>.
- Wu, Y. D., Wang, Z. Q., Luo, J. H., Cheng, J. X., Wang, Y. L., Wang, Y. D., et al. (2016). Geochemical characteristics and metallogenic mechanism analysis of the Huodehong lead-zinc deposit in northeast yunnan[J]. *Mineral. Deposits* (5), 1084–1098. (in Chinese).
- Wu, Y., Kong, Z. G., Chen, M. H., Zhang, C. Q., Cao, L., Tang, Y. J., et al. (2019). Trace element composition characteristics and indicative significance of sphalerite

- from MVT-type lead-zinc deposits in the periphery of the Yangtze plate: LA-ICPMS study[J]. *Acta Petrol. Sin.* 35 (11), 3443–3460. (in Chinese).
- Wu, Y. (2013). *The age and mechanism of large-scale metallogenesis of MVT lead-zinc deposits in Sichuan, Yunnan and Guizhou*[D]. *Doctoral Dissertation*. Beijing: China University of Geosciences, 1–152. (in Chinese).
- Yang, Q., Zhang, J., Wang, J., Zhong, W. B., and Liu, W. H. (2018a). Ore-forming fluids and isotopic geochemistry of the Tianbaoshan large lead-zinc deposit in Sichuan[J]. *Mineral. Deposits*, 816–834. (in Chinese).
- Yang, X. Y., Zhou, J. X., An, Q., Ren, H. Z., Xu, L., Lu, M. D., et al. (2018b). The formation mechanism of reduced S in the Nayongzhi lead-zinc deposit in Guizhou: NanoSIMS *in-situ* S isotope constraint[J]. *Acta Mineral.* (6), 593–599. (in Chinese).
- Ye, L., Cook, N. J., Ciobanu, C. L., Yuping, L., Qian, Z., Tiegeng, L., et al. (2011). Trace and minor elements in sphalerite from base metal deposits in south China: A LA-ICPMS study. *Ore Geol. Rev.* 39 (4), 188–217. doi:10.1016/j.oregeorev.2011.03.001
- Ye, L., Gao, W., Yang, Y. L., Liu, T. G., and Peng, S. S. (2012). Trace element composition of sphalerite from Laochang lead-zinc polymetallic deposit in Lancang, Yunnan[J]. *Acta Petrol. Sin.* 28 (5), 1362–1372. (in Chinese).
- Ye, L., Li, Z. L., Hu, Y. S., Huang, Z. L., Zhou, J. X., Fan, H. F., et al. (2016). Trace element composition of sulfide in the tianbaoshan lead-zinc deposit in sichuan: LA-ICPMS study[J]. *Acta Petrol. Sin.* 32 (11), 3377–3393. (in Chinese).
- Ye, L., Liu, T. G., and Shao, S. X. (2000). Study on the geochemistry of ore-forming fluids of the cadmium-rich zinc deposit: A case study of the Niujiaotang cadmium-rich zinc deposit in duyun. *Guizhou* (06), 597–603. (in Chinese).
- Ye, L., Pan, Z. P., and Li, C. Y. (2005). Isotopic geochemistry of Niujiaotang cadmium-rich zinc deposit in Duyun, Guizhou[J]. *Mineralogy Petrology* 25 (2), 70–74. (in Chinese).
- Ye, L., Wei, C., Hu, Y. S., Huang, Z. L., Li, Z. L., Yang, Y. L., et al. (2019). Geochemistry and resource reserve prospects of germanium[J]. *Mineral. Deposits* 4. (in Chinese).
- Yuan, B., Mao, J. W., Yan, X. H., Wu, Y., Zhang, F., Zhao, L. L., et al. (2014). The source and mechanism of mineralization of the Daliangzi lead-zinc deposit in Sichuan: Sulfur, carbon, hydrogen, oxygen, strontium isotopes and sphalerite trace elements constraints[J]. *Acta Petrol. Sin.* 30 (1), 209–220. (in Chinese).
- Zeng, X. G., Zeng, X. J., Yang, B. J., and Ye, X. Y. (1982). Geological characteristics and mineralization of vein-like lead-zinc deposits in the eastern margin of the Kangdian axis[J]. *Geol. Rev.* 28 (5), 447–452. (in Chinese).
- Zhang, C. Q., Li, X. H., Yu, J. J., Mao, J. W., Chen, F. K., Li, H. M., et al. (2008). Rb-Sr dating of sheet granule sphalerite in Daliangzi lead-zinc mine and its geological significance[J]. *Geol. Rev.* 54 (4), 532–538. (in Chinese).
- Zhang, C. Q., Liu, H., and Wang, D. H. (2015). A preliminary review on the metallogeny of Pb-Zn deposits in China[J]. *Acta Geol. Sinica-English Ed.* 89 (4), 1333–1358.
- Zhang, F. (2017). *Research on the genesis of the Tianbaoshan lead-zinc deposit in Sichuan and the background of regional metallogenetic dynamics*[D]. Beijing: Beijing: China University of Geosciences. (in Chinese).
- Zhang, J. H. (2015). *Mineral facies and genetic significance of the Daliangzi lead-zinc deposit in Huidong Sichuan*[D]. Chengdu: Chengdu University of Technology. (in Chinese).
- Zhang, Y. X., Wu, Y., Tian, G., Shen, L., Zhou, Y. M., Dong, W. W., et al. (2014). Metallogenetic age and ore-forming source of Lehong Pb-Zn deposit in yunnan: Rb-Sr and S isotope constraints[J]. *Acta Mineral. Sin.* (3), 305–311. (in Chinese).
- Zhang, Y. (2016). *The metallogenetic mechanism of fluid mixing in the Huize super-large lead-zinc deposit in the northeastern Yunnan ore concentration area*[D]. China: Kunming University of Science and Technology. (in Chinese).
- Zhang, Z. B., Li, C. Y., Tu, G. C., Xia, B., and Wei, Z. Q. (2006). The tectonic evolution background and mineralization of lead-zinc deposits in the border areas of Sichuan, Yunnan and Guizhou[J]. *Tect. Metallogenesis* 30 (3), 343–354. (in Chinese).
- Zhao, D., Han, R. S., and Ren, T. (2018). Geochemistry of fluid inclusions in the Lehong large lead-zinc deposit in northeastern Yunnan[J]. *Mineral. Deposits* 37 (5), 1018–1036. (in Chinese).
- Zhou, J. X., Huang, Z. L., Li, X. B., Zhou, G. F., Liu, S. R., Fu, S. H., et al. (2008). New evidence of germanium enrichment in galena in the Daliangzi lead-zinc deposit in Huidong, Sichuan[J]. *Acta Mineral. Sin.* 28 (4), 473–475. (in Chinese).
- Zhou, J. X., Huang, Z. L., Zhou, G. F., Jin, Z. G., Li, X. B., Ding, W., et al. (2010). Sources of ore-forming materials from hezhang tianqiao lead-zinc deposit in northwestern Guizhou: S, Pb isotopes and REE constraints[J]. *Geol. Rev.* 56 (4), 513–524. (in Chinese).
- Zhu, L. M., Luan, Sh W., and Yuan, H. H. (1994). Geological and geochemical signs of hydrothermal sedimentation of sulfide-bearing siliceous rocks in the daliangzi lead-zinc deposit, dishu[J]. *Bull. Mineralogy, Petrology Geochem.* (1), 17–18. (in Chinese).
- Zhu, L. Y., Su, W. C., Shen, N. P., Dong, W. D., Cai, J. L., Zhang, Z. W., et al. (2016). Geochemistry of fluid inclusions and sulfur isotope of lead-zinc deposits in northwestern Guizhou[J]. *Acta Petrol. Sin.* 32 (11), 3431–3440. (in Chinese).
- Zong, K., Klemd, R., Yuan, Y., He, Z., Guo, J., Shi, X., et al. (2017). The assembly of Rodinia: The correlation of early Neoproterozoic (ca. 900 Ma) high-grade metamorphism and continental arc formation in the southern Beishan Orogen, southern Central Asian Orogenic Belt (CAOB). *Precambrian Res.* 290, 32–48. doi:10.1016/j.precamres.2016.12.010